Original Article

Bayesian forces identification in cable networks with small bending stiffness

Davide Piciucco[1], Francesco Foti[1], Margaux Geuzaine[2]
and Vincent Denoël[2]

Abstract
The regular monitoring of cable forces is essential for ensuring the safety of cable structures both during construction and throughout their lifetime. This paper aims at developing a vibration-based identification procedure of the axial forces, bending stiffness, and, secondarily, the crossing point position of cable networks. A model constituted by two crossing stays having small bending stiffness and negligible sag effects is considered. The in-plane direct dynamic problem is solved both numerically and through a perturbation approach. The obtained results are compared to the outcomes of a finite element model for verification purposes. The theoretical studies are also supported by experimental tests performed on a real cable-stayed bridge (Haccourt bridge), which provide insights into the dynamics of the system showing that models of cables with small bending stiffness are more appropriate than taut string models. The inverse analysis based on non-linear Bayesian regression is developed and the closed-form asymptotic formulations are used to prove that the bending stiffness, the cable forces, and the crossing point position can be separately identified from a set of observed frequencies. The implemented procedure is then applied to the tested bridge as a proof of concept, showing that the proposed in-plane identification strategy provides satisfactory results.

Keywords
Cable network, cable force, identification, vibrations, structural health monitoring, natural frequencies, Bayesian regression

Introduction

Cable elements have a key role in important structures such as cable-stayed bridges, suspension bridges, suspended roofs, tied-arched bridges, and pedestrian walkways. They are among the main structural elements that sustain the applied loads by achieving a high level of tension. The regular monitoring of the tensile force in these cables is therefore essential for ensuring the safety of the entire structural scheme both during construction and throughout its lifetime. The detection of possible redistribution of internal forces allows to determine the actual health state of the structure and potential damages earlier than simple visual inspection.[1] The assessment of cable force can be performed using several methods based on: direct measurement of the stress in the jacks, application of strain gauges or ring load in the strands, measurement of the elongation close to the anchorage, topographic survey, and indirect measurement of the vibrations.[2] This latter method is of great interest as it is very easy to

apply, even if the free length of the cable is not accurately known. It is based on the estimation of problem parameters, for example, the cable tension, from the knowledge of the relation between the tensile force and the natural frequencies, given a set of observed frequencies. A vibration-based identification technique is discussed in this document and applied to a two-cable network. The definition of a suitable physical model for the cables is a crucial point for the accuracy of the method, therefore care is needed in making proper assumptions. One aspect that is often neglected in modeling cables (but investigated in this paper) is the

[1]Department of Civil and Environmental Engineering, Politecnico di Milano, Milano, Italy
[2]Structural and Stochastic Dynamics, Structural Engineering Division, University of Liège, Liège, Belgium

Corresponding author:
Margaux Geuzaine, NatHaz Modeling Laboratory, Cushing Hall of Engineering, University of Notre Dame, Indiana, USA.
Email: mgeuzaine@uliege.be

Figure 1. Žeželj Bridge, Novi Sad, Vojvodina, Serbia.
Source: https://structurae.net/en/structures/bridges/networkarch-
bridges. Visited in: November, 2021.

Figure 2. Cable network with two sub-spans.
Note that the bending stiffness being small, the shear force in each cable is almost negligible and does not perturb the axial force on the traverse cable.

bending stiffness effect. Indeed, simplified models based on the vibrating chord theory have been often used in the literature.[3] Nevertheless, the vibrating chord theory is not valid for the considered cable network as the natural frequencies, when plotted against the mode order, are not aligned. In this work, the bending stiffness of the cable is considered and the effect of the cable length and flexural rigidity is described on the frequency versus mode number curve.

Considered problem

The main goal of this work is to provide a simple identification tool for the estimation of cable forces in cable networks, as often used in bowstring bridges as the one depicted in Figure 1. The idealized structural model of the considered system is depicted in Figure 2. It is characterized by two crossing hangers which constitute a network of four short cable elements having lengths l_i ($i = 1 \ldots 4$), uniform bending stiffness EI, mass per unit length m, and subjected to tensile forces T_1 and T_2. The connector placed at the crossing point position is assumed to enforce the continuity of the displacement and the limited length of the cable elements makes the bending stiffness effect non-negligible at all. The sagging effect and the axial extensibility, instead, are neglected assuming the cables as highly tensioned. The end restraints are modeled as ideal fixed hinges and rollers. The boundary conditions may have an important role in cable dynamics when the effect of the bending stiffness is not negligible. Therefore, this approach is used in the paper for cable properties identification as a first tentative step to introduce the proposed model. In a future work a more involved model could be introduced by considering the end restraints as rotational and translational springs whose stiffness can be determined through Bayesian regression.
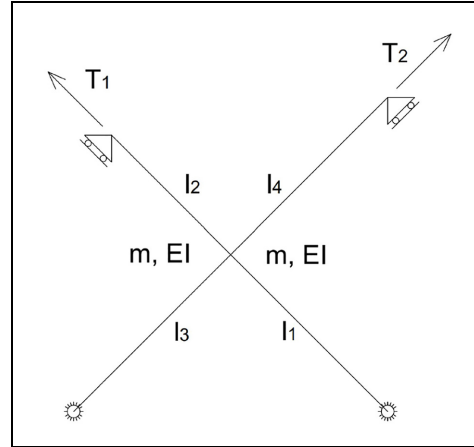
Cable networks dynamics has been an important research topic over the last few years, Caracoglia and Jones[4] developed an analytical model for a set of interconnected truss elements by using the vibrating chord theory and proposed closed-form solutions for several special cases such as networks with rigid connectors and flexible connectors. More recently, Younespour and Cheng[5,6] refined an existing analytical model of two-cable networks by including the effect of the bending stiffness in the formulation. Di et al.[7] developed a refined model for a system constituting two cables and a cross-tie, taking into account sag and cross-tie pretension effects and concluded that the latter is particularly important when the cross-tie is connected to the ground. Cross-tie flexibility and effects of cable sag were also investigated by Ahmad[8] while Jing et al.[9] developed a numerical method for the dynamic analysis of cross-tie cable systems by replacing the discrete elastic cross-tie model with an equivalent, continuously distributed, elastic model.

As an alternative to analytical modeling, the Finite Element Method (FEM) has also been used in the literature for the analysis of cable networks, especially in the past, because of their complexity. As an example, Ehsan and Scanlan[10] used finite element approaches for the solution of a three-dimensional cable problem. Cable elements can be modeled by using trusses, Bernoulli beams, or cable elements and the choice mainly depends on the adopted modeling assumptions. When dealing with long cables with negligible bending stiffness, the use of truss-type elements can be justified. On the other hand, when the bending stiffness cannot be neglected, beam type elements are preferred. More

precisely, as long as the shear deformability is negligible and the wavelength is longer than 20 cable diameters (i.e., first modes),[11] the Bernoulli beam theory can be preferred to Timoshenko models. In this work, the accuracy of the identification being more influenced by the first eigenmodes, FEM analyses of cables with small bending stiffness have been performed by using Bernoulli beam-type elements. Conversely, the analyses of cables without bending stiffness have been developed by using truss-type elements. A first difficulty in modeling cables with beam elements is related to the need to use a large density of elements near the cable ends where boundary layers develop.[12] Another concern is the numerical instability that may arise because of the small bending stiffness at the beginning of a static analysis when the structure is still unloaded and restoring forces due to geometric stiffness have not been activated yet. Instability is even obvious when truss elements are adopted, as the unloaded structure becomes a mechanism. Foti and Martinelli[13,14] proposed to use an initially imposed displacement to provide enough stiffness prior to the gradual application of the self-weight. In this work, the FEM has been used only for validation purposes and the cable tension has been applied as an initial load providing geometric stiffness to the system and avoiding instability even for zero bending stiffness.

The direct dynamic analysis and the analytical relation between the eigenfrequencies and the cable properties have been often exploited in the literature to solve inverse dynamic problems for the identification of some key parameters of isolated cable elements that are difficult to measure on-site. Cascas,[15] Gentile,[16] and Bao et al.[17] developed vibration-based methods for the computation of the cable forces that rely on the taut string model, while Geuzaine et al.[1] and Foti et al.[18] included also the small bending stiffness and the flexibility of the anchorages in the identification, exploiting linear regression and solving a non-linear optimization problem. When applied to cable networks, however, these strategies need to be adapted because of cable interactions. Just a few studies on identification techniques specifically developed for cable networks are available in the literature and a fundamental study to bridge this gap seems necessary. In recent research, Furukawa et al.[19] dealt with the in-plane and out-of-plane identification of the cable properties and axial forces in cable networks, by taking into account the axial flexibility and the bending stiffness of the crossing stays and exploiting the least-square method. A different model and method are here proposed for the monitoring of cable forces in cable networks, and the main differences and new contributions with respect to the one described in Furukawa et al.[19] are: the stays are supposed to be highly tensioned so that their axial flexibility can be neglected; Bayesian non-linear regression is used for the identification as opposed to least-square fitting. Therefore, the probability distribution of the identified properties can be obtained and prior information (e.g., from past monitoring activities) can be introduced in the process; the proposed identification tool can be used to estimate not only the forces and bending stiffness but also the crossing point location that is often difficult to evaluate on-site; the monitoring strategy here described uses mode orders; this study proposes closed-form solutions for the in-plane eigenvector and eigenfrequencies; large scale experimental results are reported in this paper and the application of the identification strategy on a real bridge is described.

Aims

Since few analytical models in the literature consider the effect of the bending stiffness in the dynamics of cable networks, this work seeks to go one step further including bending stiffness in the formulation and proposing asymptotic closed-form solutions of the in-plane dynamic problem. Further objectives include the development of an identification strategy based on non-linear Bayesian regression (NBR) for the identification of the most likely values of the bending stiffness and cable forces given some observed eigenfrequencies. Furthermore, this work aims to explore the possibility of adding the crossing point location of the networks as an additional unknown in the identification procedure. The knowledge of this latter parameter is indeed crucial since slight changes might significantly affect the natural frequencies and produce reordering of the eigenmodes because of the associated variation of the wavelengths. However, by means of other measurement techniques and the available design documentation, it is possible to start the identification with a good guess of this parameter. Therefore, the implemented strategy aims at refining the initial estimate of the connector position and providing reliable values of the cable tension and bending stiffness. The final goal is to compare the results obtained through the models to experimental tests performed on a real cable-stayed bridge and apply the implemented procedure to a real cable network. This work is indeed part of a broader project of the Service Public de Wallonie (SPW) that aims to monitor the tensions in the stays of existing bridges in Belgium.[20,21]

Organization of the text

With this purpose, the second section of the document will be devoted to the in-plane direct dynamic analysis of the cable network. The eigenvalue problem will be solved both numerically and through a perturbation

approach and the results will be compared to the FEM outcomes. Similarly to Foti et al.,[18] a closed-form asymptotic expression of the eigenfrequencies and eigenvectors will be formulated and used for understanding the set of parameters that can be separately identified from observed eigenfrequencies. The identification problem will be presented in the third section in which a description of the implemented Bayesian algorithm will be reported. The results of the application of the proposed strategy to a real cable-stayed bridge (Haccourt bridge) will be then described in the last section.

Direct analysis

The direct analysis is the evaluation of the natural frequencies and mode shapes of the cable network, once its geometry, boundary conditions, material properties, and cable tensions are known. In this section, the in-plane dynamic behavior of the cable network will be analyzed. The space continuous eigenvalue problem will be solved through a bisection algorithm and a perturbation approach, and the results will be presented and compared to the FEM outcomes. Interesting comments on the validity of the proposed solutions as well as the analysis of the main independent governing parameters will be also reported.

In-plane mathematical model

The in-plane free vibration problem can be formulated by modeling each cable constituting the network as a simply supported element with small bending stiffness. The transversal cable is assumed to be highly tensioned, therefore its restraining action is idealized through an intermediate fixed support. In this way, the in-plane dynamics of each cable can be separately investigated, leading to two uncoupled problems. Thus, let's now consider a simply supported cable of length l and mass per unit length m with an intermediate support placed at distance αl from the right support (shown in Figure 3) $\alpha \in [0; 1]$. The applied tensile force is T and the cable has a uniform small bending stiffness EI. The shear deformability, the rotational inertia effects, and sagging, can be neglected assuming the cable as slender, sufficiently extensible ($EA \gg T$), and tensioned ($T \gg mlg$), because of the small value of Irvine's parameter.[22] In the following, the problem is examined in its non-dimensional form.

A reference system is placed at the intermediate support from which two different coordinates (x_1 and x_2) depart. The non-dimensional coordinates ξ_1 and ξ_2,
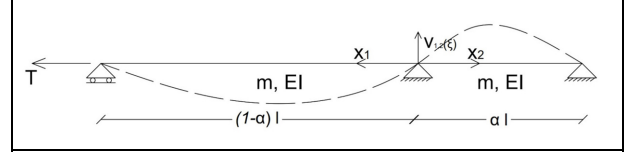
Figure 3. In-plane structural model with small bending stiffness.

and traversal displacements ν_1 and ν_2 of the two spans are expressed in Equations (1) and (2).

$$\nu_1 = \frac{\upsilon_1}{(1-\alpha)l}; \quad \nu_2 = \frac{\upsilon_2}{\alpha l} \tag{1}$$

$$\xi_1 = \frac{x_1}{(1-\alpha)l}; \quad \xi_2 = \frac{x_2}{\alpha l} \tag{2}$$

The non-dimensional bending stiffness of the two spans can be defined as:

$$\varepsilon_1 = \sqrt{\frac{EI}{T(1-\alpha)^2 l^2}}; \quad \varepsilon_2 = \sqrt{\frac{EI}{T\alpha^2 l^2}} \tag{3}$$

This choice of non-dimensional bending stiffness is the same as in Foti et al.[18] and Geuzaine et al.[1] As will be shown later with an example, practical values of non-dimensional bending stiffness ε_1 and ε_2 for the targeted applications are in between 0.04 and 0.33. Following the same derivations as in Foti et al.[18] and Geuzaine et al.,[1] the in-plane motion of the left and right subspan is respectively governed by the first and second equation of the system presented hereafter

$$\begin{cases} \varepsilon_1^2 \frac{\partial^4 \nu_1}{\partial \xi_1^4} - \frac{\partial^2 \nu_1}{\partial \xi_1^2} + \frac{\partial^2 \nu_1}{\partial \tau^2} = 0 \\ \varepsilon_2^2 \frac{\partial^4 \nu_2}{\partial \xi_2^4} - \frac{\partial^2 \nu_2}{\partial \xi_2^2} + \frac{\partial^2 \nu_2}{\partial \tau^2} = 0 \end{cases} \tag{4}$$

which is then complemented by the following set of non-dimensional boundary conditions

$$\begin{cases} \nu_1(0) = 0 & \varepsilon_1^2 \nu''_1(1) = 0 \\ \nu_1(1) = 0 & \varepsilon_2^2 \nu''_2(1) = 0 \\ \nu_2(0) = 0 & \varepsilon_1 \nu'_1(0) + \varepsilon_1 \nu'_2(0) = 0 \\ \nu_2(1) = 0 & \varepsilon_1^2 \nu''_1(0) - \varepsilon_1 \varepsilon_2 \nu''_2(0) = 0 \end{cases} \tag{5}$$

where the prime symbol indicates spatial differentiation. This list includes conditions of zero displacements at both sub-span ends, zero bending moments at the two extremities of the cable, and continuity of the slope and bending moment at the intermediate support. Note that the format chosen to enforce the continuity of the slope is multiplied by ε_1 to indicate that this continuity only holds for $EI \neq 0$. When $EI = 0$, $\varepsilon_1 = 0$, and the slope is not necessarily continuous through the

intermediate support. In the case $EI \ll Tl^2$, short boundary layers develop in the neighborhood of the support.[23] Another advantage of this formulation is that, in the limit case of $EI = 0$, only the first four B.C. suffice to pose the problem in a proper way.

General solutions for the equations in (4) can be stated in the form:

$$\nu_1(\xi_1, \tau) = \Phi_1(\xi_1) \sin (\omega_1\tau + \Theta_1) \qquad (6)$$

$$\nu_2(\xi_2, \tau) = \Phi_2(\xi_2) \sin (\omega_2\tau + \Theta_2) \qquad (7)$$

where $\Phi_1(\xi_1)$ and $\Phi_2(\xi_2)$ are the mode shapes of the cable sub-spans while ω_1 and ω_2 are the non-dimensional natural frequencies respectively referring to the left and right sub-spans. They are obtained by dividing the natural frequencies of the system, Ω, by the corresponding characteristic frequency of the taut string models, Ω_{01} and Ω_{02}—see Equations (8) and (9).

$$\omega_1 = \frac{\Omega}{\Omega_{01}} \quad \Omega_{01} = \sqrt{\frac{T}{m(1-\alpha)^2 l^2}} \qquad (8)$$

$$\omega_2 = \frac{\Omega}{\Omega_{02}} \quad \Omega_{02} = \sqrt{\frac{T}{m\alpha^2 l^2}} \qquad (9)$$

Thus, from the definition of Ω_{01} and Ω_{02}, the relation between the non-dimensional natural frequencies ω_1 and ω_2 is

$$\omega_1 = \left(\frac{1-\alpha}{\alpha}\right)\omega_2 = a\omega_2 \qquad (10)$$

with $a = (1 - \alpha/\alpha)$ being the ratio of the two sub-spans lengths.

Similarly, from their definition, the non-dimensional bending stiffness of the two sub-spans are related by:

$$\varepsilon_1 = \left(\frac{\alpha}{1-\alpha}\right)\varepsilon_2 = \frac{\varepsilon_2}{a} \qquad (11)$$

Substituting the solutions (6) and (7) in the system of governing Equation (4), one gets:

$$\begin{cases} \varepsilon_1^2 \frac{\partial^4 \Phi_1(\xi_1)}{\partial \xi_1^4} - \frac{\partial^2 \Phi_1(\xi_1)}{\partial \xi_1^2} - \omega_1^2 \Phi_1(\xi_1) = 0 \\ \varepsilon_2^2 \frac{\partial^4 \Phi_2(\xi_2)}{\partial \xi_2^4} - \frac{\partial^2 \Phi_2(\xi_2)}{\partial \xi_2^2} - \omega_2^2 \Phi_2(\xi_2) = 0 \end{cases} \qquad (12)$$

after some straightforward computations. Substitution of (6) and (7) in the set of boundary conditions (5) then gives:

$$\begin{cases} \Phi_1(0) = 0 & \varepsilon_1^2 \Phi''_1(1) = 0 \\ \Phi_1(1) = 0 & \varepsilon_2^2 \Phi''_2(1) = 0 \\ \Phi_2(0) = 0 & \varepsilon_1 \Phi'_1(0) + \varepsilon_1 \Phi'_2(0) = 0 \\ \Phi_2(1) = 0 & \varepsilon_1^2 \Phi''_1(0) - \varepsilon_1 \varepsilon_2 \Phi''_2(0) = 0 \end{cases} \qquad (13)$$

General solutions of the Equations (12) are:

$$\Phi_1(\xi_1) = \varphi_1 \sin(z_1\xi_1) + \varphi_2 \cos(z_1\xi_1) + \varphi_3 e^{-z_2\xi_1} \\ + \varphi_4 e^{-z_2(1-\xi_1)} \qquad (14)$$

$$\Phi_2(\xi_2) = \varphi_5 \sin (z_3\xi_2) + \varphi_6 \cos (z_3\xi_2) + \varphi_7 e^{-z_4\xi_2} \\ + \varphi_8 e^{-z_4(1-\xi_2)} \qquad (15)$$

with $z_j(j = 1, 2)$ and $z_i(i = 3, 4)$ being functions of the non-dimensional frequencies, ω_1 and ω_2, and the non dimensional bending stiffness parameters, ε_1 and ε_2. They indeed read

$$z_j(\omega_1, \varepsilon_1) = \frac{1}{\varepsilon_1\sqrt{2}} \sqrt{(-1)^j + \sqrt{1 + (2\varepsilon_1\omega_1)^2}} \qquad (16)$$

$$z_i(\omega_2, \varepsilon_2) = \frac{1}{\varepsilon_2\sqrt{2}} \sqrt{(-1)^i + \sqrt{1 + (2\varepsilon_2\omega_2)^2}} \qquad (17)$$

Note that for stay-cables, ε_1 and ε_2 are so close to zero that z_2 and z_4 reach high positive values.

Substitution of the solutions (14) and (15) in the boundary conditions (13) leads to the following algebraic eigenvalue problem:

$$\boldsymbol{B}(\omega_2, \varepsilon_2, a) \boldsymbol{\varphi} = 0 \qquad (18)$$

The 8×8 matrix $\boldsymbol{B}$ contains 64 elements which depend on thhe crossing ratio a, the non-dimensional bending stiffness ε_2 and the non-dimensional frequency ω_2 only. Indeed, ω_1 and ε_1 are functions of ω_2 and ε_2 through the relations (10) and (11). The entries of the boundary conditions matrix $\boldsymbol{B}$ are reported in Appendix A. The column vector $\boldsymbol{\varphi}$ lists the eight integration constants $\boldsymbol{\varphi} = (\varphi_1, \ldots, \varphi_8)$ of the solutions (14) and (15).

Numerical solution

The nontrivial solutions, $(\omega_{2,k}; \boldsymbol{\varphi}_k)$; with $k \in \mathbb{N}^+$, of the algebraic eigenvalue problem (18) can be computed by considering the following characteristic equation:

$$\det \boldsymbol{B}(\omega_2, \varepsilon_2, \alpha) = 0 \qquad (19)$$

Exact analytical expressions can be derived for Equation (19) in some simple cases, for example, two sub-spans of equal lengths. For other configurations though, this equation can be solved through a suitable root-finding algorithm.[18] To do so, in this paper, a bisection algorithm has been implemented in MATLAB. In the sequel, the numerical results given by this numerical method for the eigenfrequencies and the eigenmodes will be presented and compared to the outcomes of a finite element model and a closed-form expression obtained through the application of a perturbation approach.

Perturbation approach

Such an analytical formula is extremely useful in the implementation of vibration-based identification procedures because it helps to determine the independent groups of parameters that can be identified separately from given eigenfrequencies. For the moment, however, exact solutions of the eigenvalue problem (18) exist for some simple cases only. Taking cue from Foti et al.[18] and Geuzaine et al.,[1] a second-order accurate asymptotic expression is therefore developed in this section. This formulation is derived by means of a standard perturbation approach which consists in searching for a solution of the eigenvalue problem (18) in the form of the following regular expansion:

$$\omega = \omega_{(0)} + \omega_{(1)}\varepsilon_2 + \omega_{(2)}\varepsilon_2^2 + o(\varepsilon_2^3) \quad (20)$$

$$\boldsymbol{\varphi} = \boldsymbol{\varphi}_{(0)} + \boldsymbol{\varphi}_{(1)}\varepsilon_2 + \boldsymbol{\varphi}_{(2)}\varepsilon_2^2 + o(\varepsilon_2^3) \quad (21)$$

Substitution of Equation (20) in the expression of z_1, z_2, z_3 and z_4, that is, Equations (16) and (17), and subsequent Taylor expansion of entries of the $\boldsymbol{B}$ matrix in the neighborhood of $\varepsilon_2 = 0$ leads to the following second order accurate expression of $\boldsymbol{B}$:

$$\begin{aligned} \boldsymbol{B} = {} & \boldsymbol{B}_{(0)}(\omega_{(0)}) + \boldsymbol{B}_{(1)}(\omega_{(0)}, \omega_{(1)})\varepsilon_2 \\ & + \boldsymbol{B}_{(2)}(\omega_{(0)}, \omega_{1(1)}, \omega_{(2)})\varepsilon_2^2 + o(\varepsilon_2^3) \end{aligned} \quad (22)$$

where $\boldsymbol{B}_{(0)}$, $\boldsymbol{B}_{(1)}$ and $\boldsymbol{B}_{(2)}$ are respectively the zeroth order, the first order, and the second order $\boldsymbol{B}_{(n)}$ matrices whose entries are reported in Appendix A.

Replacing the second order expressions of $\boldsymbol{B}$ and φ, namely Equations (22) and (21), in the eigenvalue problem (18), one gets the following equation:

$$\left(\boldsymbol{B}_{(0)} + \boldsymbol{B}_{(1)}\varepsilon_2 + \boldsymbol{B}_{(2)}\varepsilon_2^2\right)\left(\boldsymbol{\varphi}_{(0)} + \boldsymbol{\varphi}_{(1)}\varepsilon_2 + \boldsymbol{\varphi}_{(2)}\varepsilon_2^2\right) = 0 \quad (23)$$

The individual vanishing of the terms at different powers in ε_2 leads to the definition of three different problems collected in the system (24).

$$\begin{cases} \text{ord}\left(\varepsilon_2^0\right) : \boldsymbol{B}_{(0)}\,\boldsymbol{\varphi}_{(0)} = 0 \\ \text{ord}\left(\varepsilon_2^1\right) : \boldsymbol{B}_{(0)}\,\boldsymbol{\varphi}_{(1)} + \boldsymbol{B}_{(1)}\,\boldsymbol{\varphi}_{(0)} = 0 \\ \text{ord}\left(\varepsilon_2^2\right) : \boldsymbol{B}_{(0)}\,\boldsymbol{\varphi}_{(2)} + \boldsymbol{B}_{(1)}\varphi_{(1)} + \boldsymbol{B}_{(2)}\,\boldsymbol{\varphi}_{(0)} = 0 \end{cases} \quad (24)$$

The first equation represents the leading order problem, whose solutions are associated to the unperturbed problem of the in-plane vibrations of a net of cables without bending stiffness. The second and the third equations are respectively the first and the second order problems. The overall system can be solved for the coefficients $\omega_{(n)}$ and eigenvectors $\boldsymbol{\varphi}_{(n)}$ $n = 0, 1, 2$ through a cascade approach, starting from the leading order problem and then searching for the first and second order corrections. Additional details of the procedure are reported in Appendix B. The proposed method

allows formulating the following second-order accurate closed-form expression for the natural frequencies:

$$\omega_k = \frac{k\pi}{a}\left(1 + \frac{\varepsilon_2}{2a} + \frac{1 + 2k^2\pi^2 + k\pi\cot\left(\frac{k\pi}{a}\right)}{4a^2}\varepsilon_2^2\right) \quad (25)$$

or

$$\omega_k = k\pi\left(1 + \frac{\varepsilon_2}{2} + \frac{1 + 2k^2\pi^2 + k\pi\cot(k\pi a)}{4}\varepsilon_2^2\right) \quad (26)$$

The proposed solution is valid as long as $\varepsilon_2 \ll 1$. When this happens, Equations (25) and (26) show that the in-plane eigenfrequencies are a function of two non-dimensional parameters: the crossing point position α, through $a = (1 - \alpha/\alpha)$, and the bending stiffness ε_2, or equivalently ε_1 and ε_2, through $\varepsilon_1 = \varepsilon_2/a$. Moreover, these pairs of dimensionless parameters turn out to be separately identifiable as there are no symmetric permutations possible in the proposed asymptotic formulas.[1] For instance, when increasing the bending stiffness, variations of the right sub-span length (i.e., α) do not produce any compensation in the values of the eigenfrequencies. For symmetry reasons, though, the eigenfrequencies are insensitive to the swapping of the sub-span lengths. As evidence, replacing a with $1/a$ and ω with ω/a gives the same set of dimensional frequencies. In consequence, the pairs of parameters considered in this paragraph can be uniquely identified from observed frequencies, provided that α is limited between 0 and 0.5.

Results

In addition to the numerical and closed-form asymptotic solutions, the dynamic analysis of a stay cable with small bending stiffness is performed by using a finite element model. The cables are represented by Bernoulli beam elements having a circular cross-section, and each sub-span is discretized with 20 elements. The number of elements is indeed more than enough to capture the first few modes that are useful for the identification problem (about 10 modes).[24] The intermediate and the end restraints are fixed hinges and the only applied load is the cable force that is provided as an initial load for the eigenvalue analysis. This load is applied as static internal member forces due to external loads, providing geometric stiffness in linear stiffness. Therefore, the static configuration is not stress free. The software used for the simulations is *MIDAS Gen 2020*. The non-dimensional frequencies ω_k obtained through FEM are listed in Table 1 together with the ones obtained with the numerical solution of (19) and the perturbation approach for a cable having non-dimensional bending stiffness parameters comparable

Table 1. In-plane circular eigenfrequencies of the cable with $\varepsilon_1 = 0.059$ and $\varepsilon_2 = 0.108$. In parenthesis is the relative error with respect to the numerical results.

Circular frequencies	Numerical outcomes (–)	Perturbation approach (–)	FEM results (–)
ω_1	1.7864	1.7854 (0.057%)	1.7730 (0.754%)
ω_2	3.4438	3.4489 (0.147%)	3.4178 (0.755%)
ω_3	3.8249	3.8133 (0.305%)	3.7962 (0.751%)
ω_4	6.0119	6.0372 (0.422%)	5.9665 (0.754%)
ω_5	7.9226	8.0181 (1.205%)	7.8617 (0.769%)
ω_6	8.8640	9.0101 (1.649%)	8.7959 (0.768%)

FEM: finite element method.
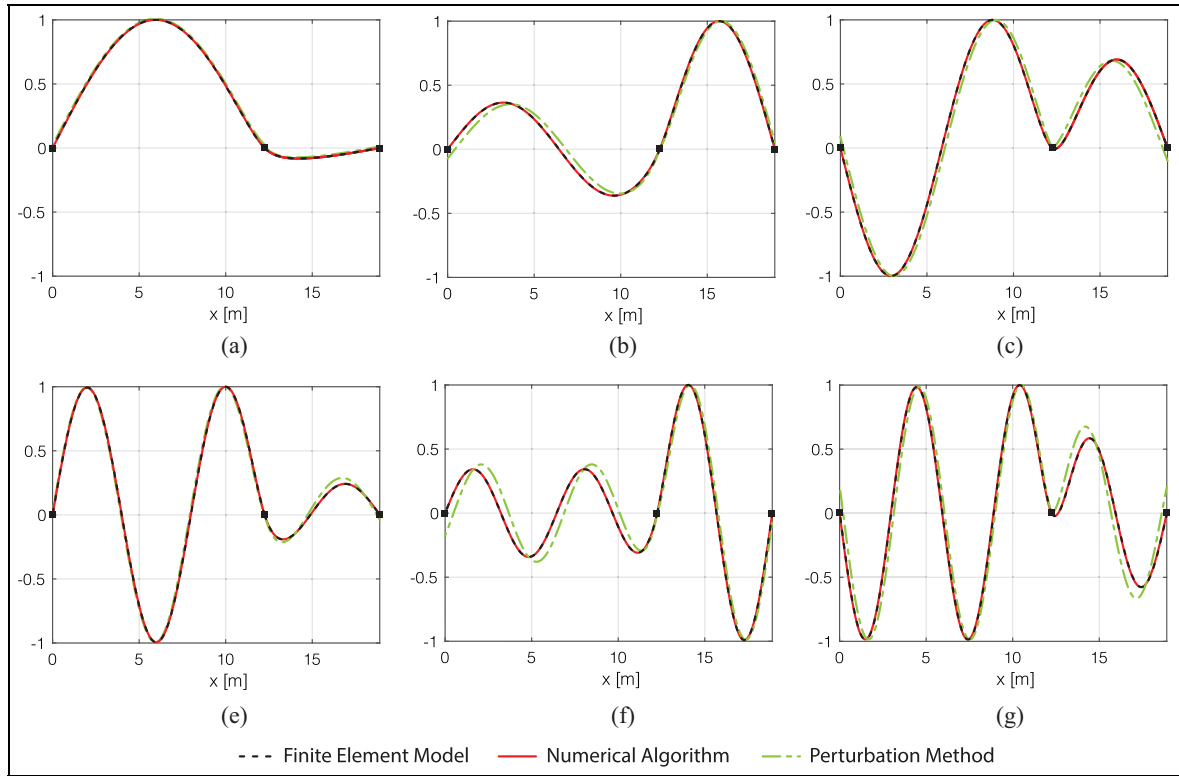
Figure 4. Mode shapes for the in-plane problem of a cable network having $\varepsilon_1 = 0.059$ and $\varepsilon_2 = 0.108$. (a) Mode 1, (b) Mode 2, (c) Mode 3, (d) Mode 4, (e) Mode 5, and (f) Mode 6.

to the ones observed in the tested bridge described later ($\varepsilon_1 = 0.059$ and $\varepsilon_2 = 0.108$, i.e., $\alpha = 0.35$, $a = 1.86$). The relative errors with respect to the numerical results are reported in parenthesis.

The corresponding eigenmodes are also depicted in Figure 4. The red lines and the dashed black lines represent the numerical mode shapes and the FEM mode shapes, respectively. It is worth noting that there is a coupling between the eigenmodes of the left and right sub-spans, that would not have been reproduced by a taut string model. In this case, all the modes deform the whole cable length and this effect is associated with the small bending stiffness as it constitutes an additional degree of connection between the vertical in-plane motions of the two sub-spans. The seemingly perfect matching between these mode shapes and the errors lower than 1% on the eigenfrequencies for the numerical and the finite element results allow to verify the modeling assumptions.

Larger differences can be noted for the fifth and sixth eigenfrequencies when they are given by the perturbation approach. These errors are reflected in the

Table 2. In-plane circular eigenfrequencies of the cable with $\varepsilon_1 = 0.012$ and $\varepsilon_2 = 0.022$. In parenthesis is the relative error with respect to the numerical results.

Circular frequencies	Numerical results (–)	Perturbation approach (–)
ω_1	1.7167	1.7166 (0.001%)
ω_2	3.1810	3.1811 (0.003%)
ω_3	3.4433	3.4430 (0.008%)
ω_4	5.1774	5.1772 (0.004%)
ω_5	6.4071	6.4070 (0.002%)
ω_6	6.9419	6.9413 (0.009%)

mode shapes which are computed with the asymptotic expressions of Equation (21) and represented by green dashed lines in Figure 4. Given that the perturbation approach yields approximate results for the eigenfrequencies, it is not possible to fulfill all boundary conditions in a simultaneous way. Non-zero displacements at the extremities of the cable, as well as discontinuities of slope and curvature at the intermediate support can therefore be observed in these mode shapes when compared to the numerical ones.

Nevertheless, the second-order asymptotic solution provides approximate results whose errors are proportional to ε^3. The accuracy of these asymptotic results therefore increases as the bending stiffness of the cables reduces. For example, if one considers a second case with reduced values of bending stiffness parameters (1/5 of the previous ones) $\varepsilon_1 = 0.012$ and $\varepsilon_2 = 0.022$, the errors in the computed eigenfrequencies are reduced by one order of magnitude as shown in Table 2. Moreover, the asymptotic mode shapes depicted in Figure 5 are much closer to the numerically computed ones and do not show any significant discontinuity at the boundary layer nor significant displacement at the support. This is because both the eigenfrequencies and eigenvectors are better approximated by the closed-form expressions obtained through the perturbation method.

Inverse problem analysis

The knowledge of all the parameters involved in the problem is of paramount importance to capture the real dynamic behavior of the cable network. Moreover,
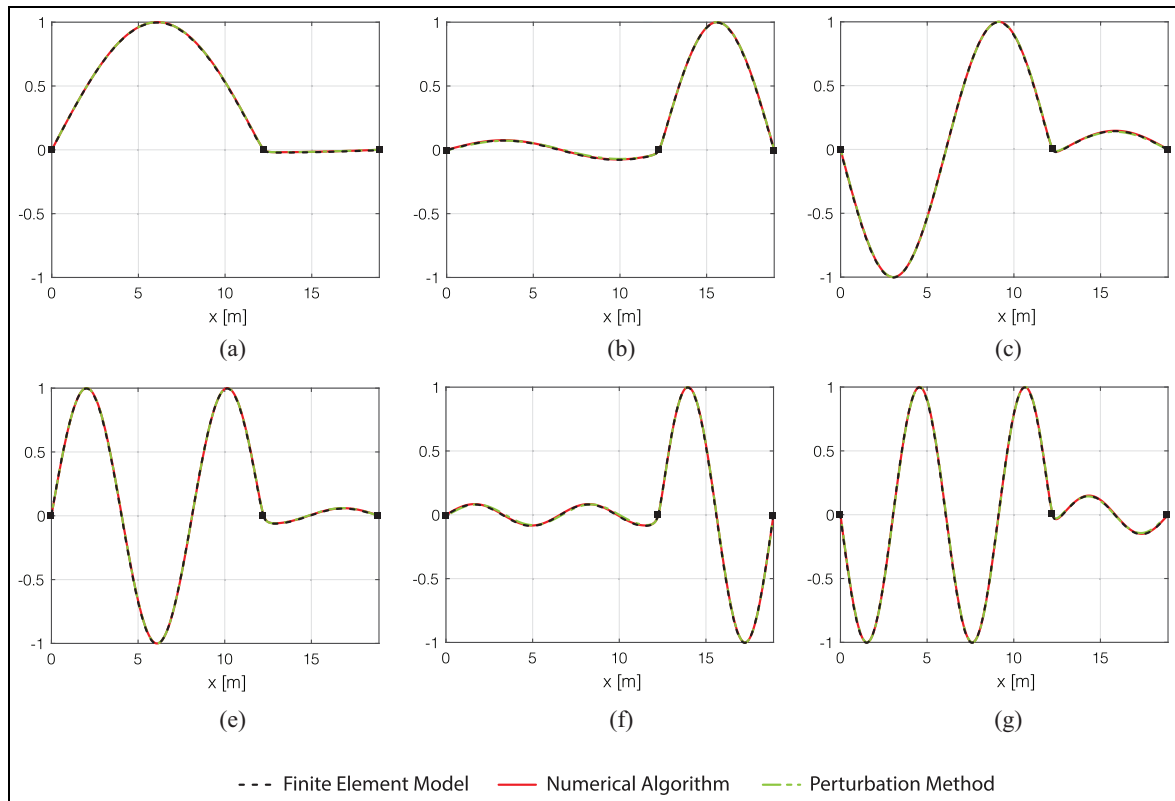
Figure 5. Mode shapes for the in-plane problem of a cable network having $\varepsilon_1 = 0.012$ and $\varepsilon_2 = 0.022$. (a) Mode 1, (b) Mode 2, (c) Mode 3, (d) Mode 4, (e) Mode 5, and (f) Mode 6.

simple identification procedures aimed at estimating the tensile forces of the stays are extremely important in monitoring existing cable structures since they provide information both on the current health condition and on the evolution of the state of the structures.[25,26] In this section the implementation of an identification procedure based on the Bayesian inference is addressed. More specifically, the procedure involves the identification of some unknown independent parameters starting from a set of observed eigenfrequencies $\Omega_k^*(k=1,\ldots,N)$, through a NBR.

Non-linear Bayesian regression

The NBR is based on the same model as the classical frequentist approach[27]

$$y = f(x, \boldsymbol{\beta}) + \varepsilon \qquad (27)$$

The model relates the dependent variables y to the independent variables x through the non-linear function $f(x, \boldsymbol{\beta})$, $\boldsymbol{\beta}$ being the vector of parameters to be identified. In this specific case of Non-linear regression applied to vibration-based identification procedures the eigenfrequencies Ω_k act as dependent variables that can be expressed as a function of the mode orders k, through the independent parameters on which the natural frequencies depend $(T, EI\ldots)$. The error ε is assumed to be normally distributed with zero mean and constant variance σ^2. The goal of the procedure is to find the coefficients $\boldsymbol{\beta}$ that best explain the observed eigenfrequencies Ω_k^*. While the classical frequentist regression searches for a single "best" value of $\boldsymbol{\beta}$ that minimizes the residual sum of the squares Equation (28)[28] (being Ω_k^* the observed frequencies and N the number of frequencies), the Bayesian regression determines the joint posterior distribution of the model parameters, then maximizes their likelihood.

$$\Phi(\beta) = \frac{1}{N} \sum_{k=1}^{N} (\Omega_k - \Omega_k^*)^2 \qquad (28)$$

One of the main advantages of the latter compared to the former is that if prior knowledge of the model parameters is available from past monitoring activities, it can be included in the procedure through the so called prior of $\boldsymbol{\beta}$ ($p(\boldsymbol{\beta})$). In this specific application, a non-informative constant is used since it is assumed that estimates of the modal parameter will not be available. The Bayesian regression allows also to quantify the uncertainty about the model as its result is a joint distribution of the parameters given the prior. For instance, a low quantity of data would be reflected in a more spread out posterior distribution which indicates greater uncertainty in the model. The

key point of the Bayesian regression is the Bayes' theorem which states that joint posterior $p(\boldsymbol{\beta}|y)$ is proportional to the product of the likelihood $p(y|\boldsymbol{\beta})$ and the joint prior distribution $p(\boldsymbol{\beta})$:

$$p(\boldsymbol{\beta}|y) = \frac{p(y|\boldsymbol{\beta})p(\boldsymbol{\beta})}{p(y)} \propto p(y|\boldsymbol{\beta})p(\boldsymbol{\beta}) \qquad (29)$$

The goal of the procedure is to compute the joint posterior distribution $p(\boldsymbol{\beta}|y)$ of the model parameters. This requires to solve intractable integrals and therefore sampling techniques based upon Markov Chain Monte Carlo methods are preferred to analytical equations. These methods allow to compute the posterior, by drawing samples from the posterior itself.

One of the Monte Carlo sampling algorithms is the Metropolis-Hastings (MH)[29] which is based on the following steps (note that the superscript "0" denotes the initial values of the unknown parameters, while the superscripts "i" and "$i-1$" indicate the accepted samples at iteration i and $i-1$):

1. It starts by initializing the sample value for each random variable $\boldsymbol{\beta}^{(0)}$;
2. It samples from a proposal distribution $q(\boldsymbol{\beta}^{(i)}, \boldsymbol{\beta}^{(i-1)})$ a candidate value $\boldsymbol{\beta}^{(\text{cand})}$;
3. Then it computes the acceptance probability $\tau(\boldsymbol{\beta}^{(\text{cand})}|\boldsymbol{\beta}^{(i-1)})$ through the acceptance function $r(\boldsymbol{\beta}^{(\text{cand})}, \boldsymbol{\beta}^{(i-1)})$ based on the proposal distribution and the full joint density of the parameters $\pi(\boldsymbol{\beta})$.

$$r(\boldsymbol{\beta}^{(\text{cand})}, \boldsymbol{\beta}^{(i-1)}) = \frac{q(\boldsymbol{\beta}^{(i-1)}|\boldsymbol{\beta}^{(\text{cand})})\pi(\beta^{(\text{cand})})}{q(\boldsymbol{\beta}^{(\text{cand})}|\boldsymbol{\beta}^{(i-1)})\pi(\boldsymbol{\beta}^{(i-1)})} \qquad (30)$$

If the proposal distribution is symmetric, the acceptance function become just the ratio of the full joint PDF of the variables $\boldsymbol{\beta}$ that, exploiting the Bayes' theorem, is proportional to the prior multiplied by the likelihood. Therefore, if one uses a non-informative prior, the acceptance function is just the ratio of the likelihoods computed at $\boldsymbol{\beta}^{(\text{cand})}$ and $\boldsymbol{\beta}^{(i-1)}$:

$$r(\boldsymbol{\beta}^{(\text{cand})}, \boldsymbol{\beta}^{(i-1)}) = \frac{p(y|\boldsymbol{\beta}^{(\text{cand})})}{p(y|\boldsymbol{\beta}^{(i-1)})} \qquad (31)$$

$$\tau(\boldsymbol{\beta}^{(\text{cand})}|\boldsymbol{\beta}^{(i-1)}) = \min[1, r(\boldsymbol{\beta}^{(\text{cand})}, \boldsymbol{\beta}^{(i-1)})] \qquad (32)$$

4. The algorithm then draws a uniform random number u between 0 and 1. This step introduces randomness in the procedure, with u being used as a discriminating factor in the next step for accepting the candidate value. As a consequence, the accepted samples as well as the rate of convergence may be slightly different when repeating the

identification. Nevertheless, the algorithm is always able to reach the optimum of the minimization problem and the same final estimates even for noised frequencies as it will be demonstrated later in Figure 13;

5. The current value $\boldsymbol{\beta}^{(\text{cand})}$ is then accepted or rejected depending on the value of the acceptance probability:

$$\begin{cases} \text{if } u < \tau \Rightarrow \text{accepted} & \boldsymbol{\beta}^{(i)} \leftarrow \boldsymbol{\beta}^{(\text{cand})} \\ \text{if } u \geq \tau \Rightarrow \text{rejected} & \boldsymbol{\beta}^{(i)} \leftarrow \boldsymbol{\beta}^{(i-1)} \end{cases} \tag{33}$$

6. Once the established number of samples has been computed the algorithm creates a histogram which approximates the prior distribution of $\boldsymbol{\beta}$. It is worth noting that the drawn samples depend on an initial value $(\boldsymbol{\beta}^{(0)})$. Thus the samples associated with an initial transient phase called "burn-in period" (time required for the Markov chain to reach its steady state) should be discarded for the construction of the histogram.

The computed joint posterior distribution can be then used to estimate, by integrating the marginal posteriors, the mean values, and the credible intervals (CIs) associated with each model parameter. The Bayesian non-linear regression indeed, provides not only a final estimate of the unknowns, that is the mean (or most probable) value, but also a range of possible values for the model parameters, that is the CI. Several definitions of the CI are available in the literature, two examples are the Equal Tail CI and the Highest Posterior Density (HPD) CI (see Hespanhol et al.[30]). Graphical representations of CIs computed on symmetric and skewed posteriors are shown in Figure 6. In this work, the Equal Tail definition will be adopted and the upper and lower limits of the CI will be computed adding and subtracting to the mean value twice the standard deviation. Generally speaking, it represents the interval associated with the 95% probability that the true value falls within this range, given the observed data, and it is a measure of the accuracy of the model. This interval indeed shrinks as the number of available data increases and the noise decreases.
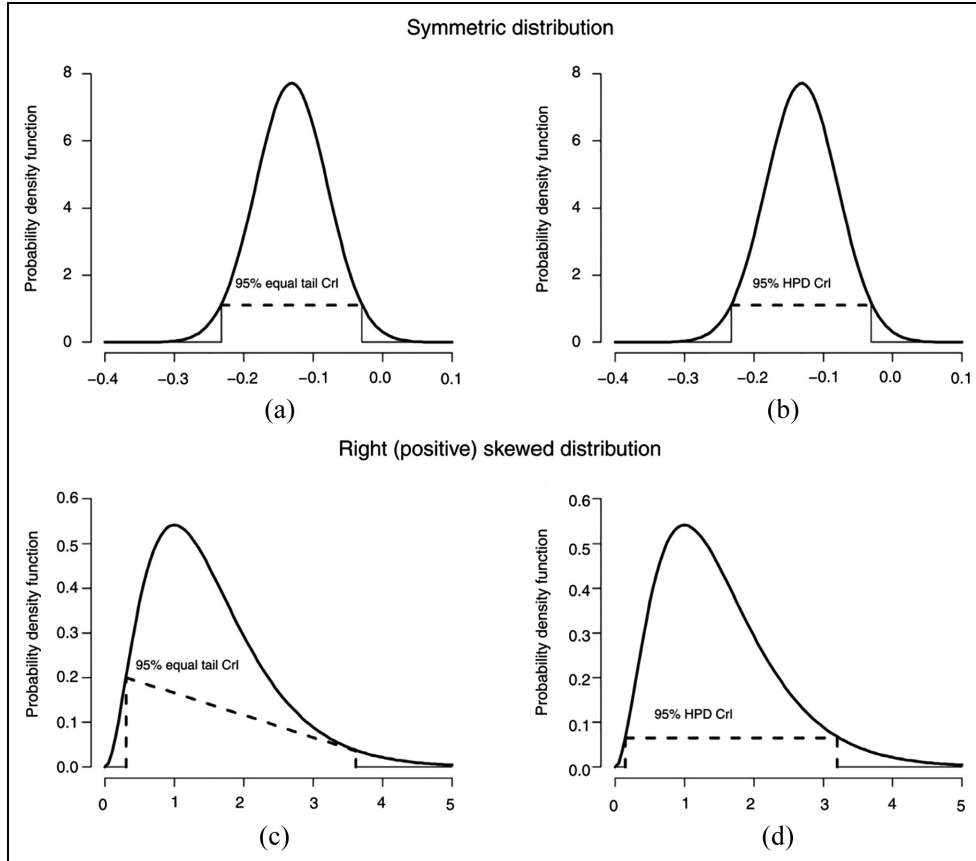
Figure 6. Examples of Equal Tail and highest posterior density credible intervals
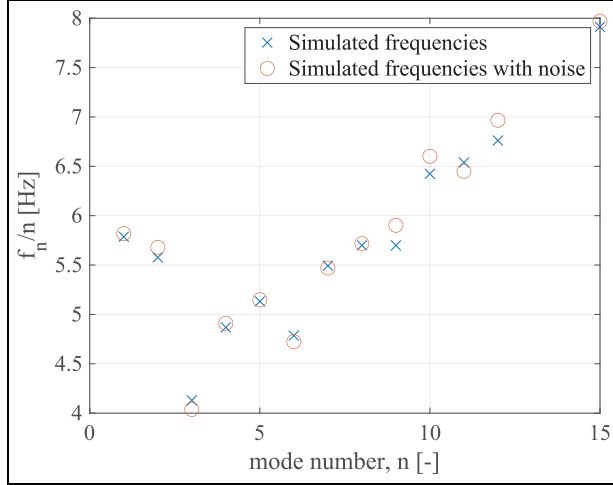
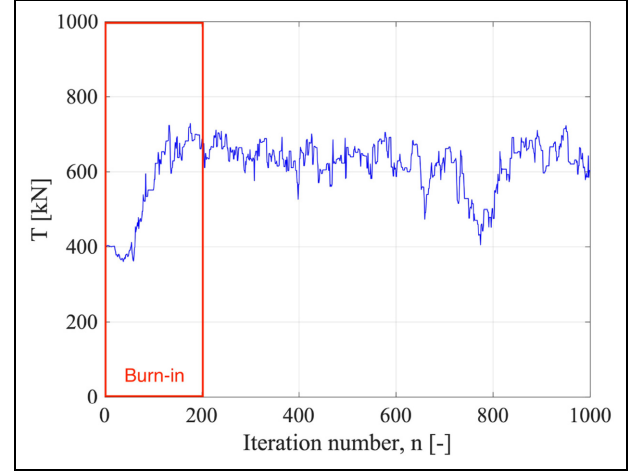**Figure 7.** Simulated in-plane frequencies with 1% noise (Numerical values: see Table 3).

Figure 8. Example of samples of the in-plane problem.

Description of the identification algorithm

In this section a general description of the identification algorithm used for the in-plane inverse analysis of the studied cable network is reported, more details can be found in the following sections. As already mentioned, the identification is based on a NBR which allows to determine the most likely values of the governing parameters which explain the observed data.

The Bayesian algorithm starts with a set of natural frequencies that in a monitoring situation are collected on-site. Note that the proposed identification algorithm relies on prior knowledge of the mode orders and is sensitive to possible missing frequencies. The technique is still not fully automated and some manual operations are necessary to ensure that the eigenfrequencies are provided in the correct order without missing data. However, some tools already studied in statistics, such as *missing data imputation*,[31] could be used to make the process fully automated. Before applying the algorithm to real data, we will validate it with synthetic data, which offers a (ground-truth) reference solution. To do so, simulated frequencies are corrupted by a normal distribution of noise having zero mean and user-definable variance. The number of simulated eigenfrequencies or data to be used in the problem depends on the level of accuracy that one wants to achieve. Increasing the number of observed data, the uncertainty of the joint PDF of the parameters is expected to decrease. Examples of simulated eigenfrequencies with the noise having a coefficient of variation (CoV) equal to 1% are reported in Figure 7.

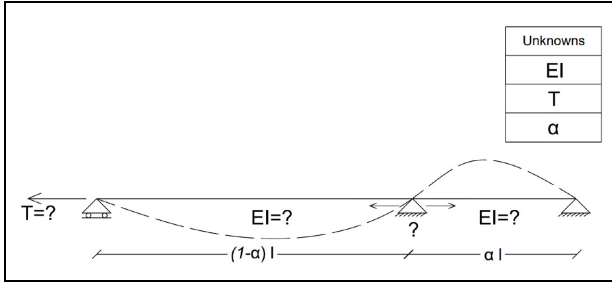Once the parameters to be identified are known, the MH algorithm requires the setting of an initial value for each of the unknowns. Then, upper-bounds and lower-bounds are defined to fix the set of values that should be explored for each of the unknowns. The choice of these limits depends on the level of knowledge that one has on the unknown parameters. In this specific application, the tensile forces and the bending stiffness are expected to vary between one-tenth and ten times the initial nominal values while specific upper bounds for the crossing point location will be discussed in the following.

When the frequencies have been simulated and all the settings defined, the algorithm starts generating samples of the unknown parameters in the previously defined intervals. For each sample, the algorithm computes the associated natural frequencies and the acceptance function as the ratio of the likelihoods of the eigenfrequencies given the candidate parameters. Depending on the value of the acceptance function the candidates are then accepted or rejected. Any candidate falling out of the bounds is immediately rejected.

The sampling procedure is repeated up to the maximum established number of iterations. One example of iterative sampling is shown in Figure 8 for the estimate of the cable tension of the in-plane problem. It is worth noting that the process strongly depends on the assigned initial value. In this example, a transient initial branch which lasts about 200 iterations is needed to converge toward more likely values. This initial part is called Burn-in > zone and has to be discarded by neglecting a proper number of iterations at the beginning of the sampling. This latter has to be calibrated depending on the problem that is addressed.

The stationary part of the iterations can be used to build histograms of the unknown parameters that approximate the objective PDF. The obtained

Figure 9. In-plane identification problem.

Table 3. Nominal values of the inverse problem.

m (kg/m)	l (m)	T (kN)	EI (kN m^2)	α (–)
34.94	18.90	640	331.37	0.35

Table 4. Initial values of the unknown parameters.

T_0 (kN)	EI_0 (kN m^2)	α_o (–)
400	400	0.31

posteriors are then used to get the estimate of the parameters as the mean of the samples while the CI is computed through Equation (35) from the standard deviation of the samples. Note that the Bayesian method is in principle devoted to the determination of a most probable value. However, since the obtained distributions are more or less symmetric in this application, the mean values (34) are used as parameter estimates.

$$\beta_{est} = \text{mean}[\beta_i] \qquad (34)$$

$$CI = \beta_{est} \pm 2\sigma \qquad (35)$$

In the following, the in-plane identification problem will be addressed. It tries to identify from observed eigenfrequencies the axial force, the bending stiffness, and the crossing point location along each cable constituting the network. The identification of this last unknown parameter is of particular interest when the position of the connectors along the cables cannot be easily measured on-site.

In-plane identification

Let's assume that the total length l and the mass per unit length m of the cable in Figure 9 are known. Given a set of N in-plane experimentally measured natural frequencies Ω_k, the objective is the identification of the cable tension T, the bending stiffness EI, and the sub-span length αl.

The reference values in Table 3, can be used to simulate a set of 15 eigenfrequencies through the numerical method previously described. The obtained data are then corrupted by normally distributed noise having a CoV equal to 1%. At this point, the non-linear regression can be applied to the simulated frequencies to try to get back the reference nominal values.

Before applying the MH sampling procedure, the initial values of the unknown variables are set far enough from the actual ones as in Table 4.

The upper and lower bounds of the explorable intervals for the bending stiffness and the cable force are

defined as one-tenth and ten times the initial values. The upper bound of the α parameter instead, following the insensitivity to the swapping of the sub-span lengths observed also in the asymptotic closed-form solution, has to be limited to 0.5 to get just one of the two symmetric solutions. The whole set of samples obtained after 5000 jumps (iterations) is depicted in Figure 10(a), (c), and (e). It is worth noting that the algorithm takes about 100 jumps to converge toward more likely values of the tensile force, bending stiffness, and crossing point location. In the stationary part, the accepted samples assume values contained in a restricted band whose amplitude depends on the uncertainties of the measured data. The Burn-in period is set conservatively to 2000 iterations, as the length of the non-stationary branch to be neglected is defined before the sampling. A narrower interval may be used if one looks at the samples a posteriori (100 iterations). Then, the accepted samples can be plotted in a histogram that approximates the objective joint PDF of the model parameters.

The obtained distributions for each model parameter are plotted in Figure 10(b), (d), and (f). The dashed black vertical lines represent the nominal values of the unknowns listed in Table 3 while the CIs are depicted with blue vertical lines. The three histograms can be approximated by bell-shaped distributions whose mean values are very close to the nominal ones. The final estimates are listed in Table 5 along with the associated errors that are very close to zero. Overall, being also the nominal values contained inside the CIs, the algorithm can be considered to provide satisfactory results. The best-estimated parameter is the bending stiffness since the final result has only 0.18% error. Looking just at the final estimate, however, could be limiting when applying a Bayesian approach. Conversely, it is useful to look at the obtained distributions, noting a sharp peak in the α histogram that is due to a low value of the standard deviation of the samples. The CoV of α is indeed much lower than the ones of the other two parameters: 0.96% compared to 4.5% and 9.4% for EI and T respectively. Therefore
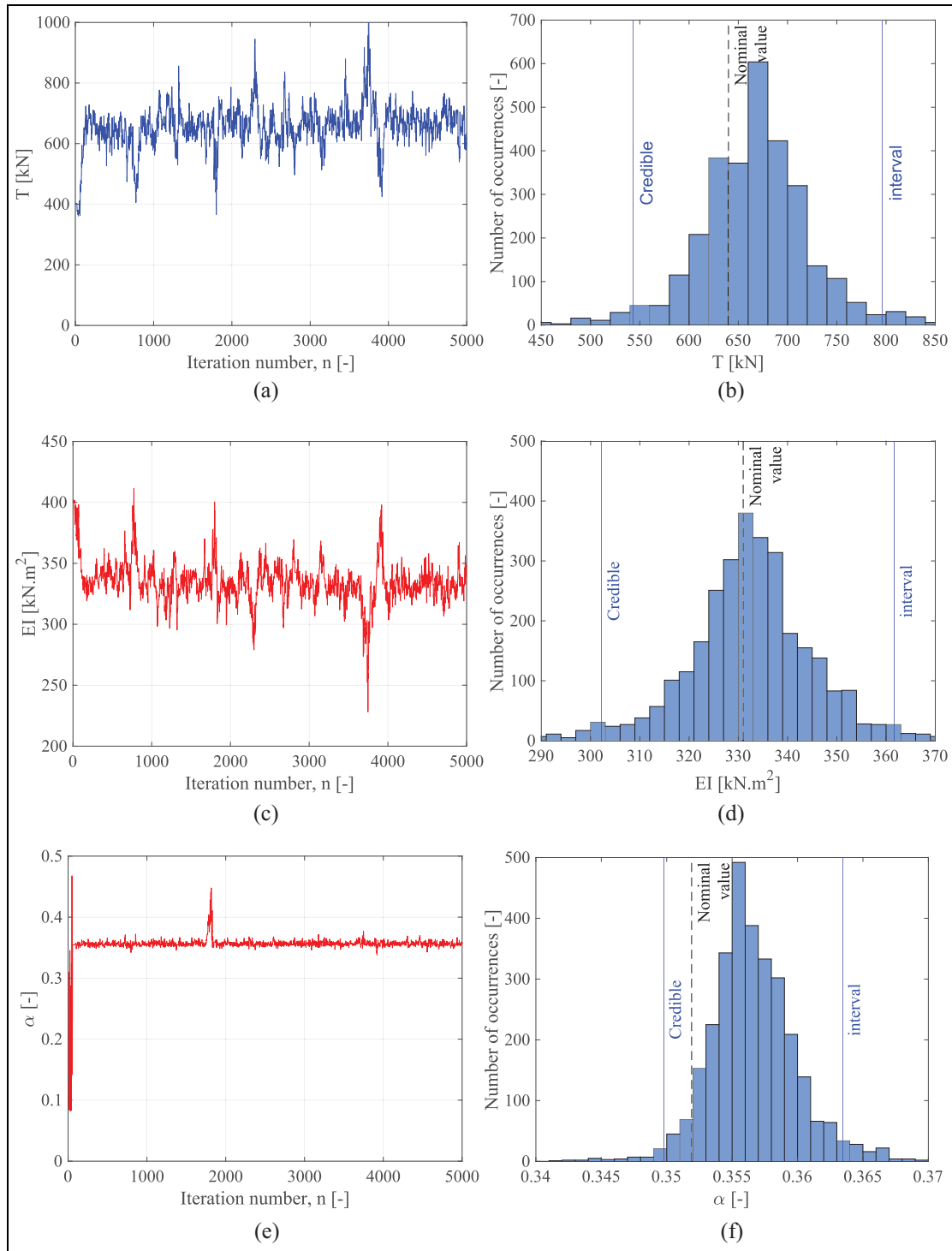
Figure 10. In-plane identification: iterations and obtained histograms. (a) tensile force samples, (b) tensile force histogram, (c) bending stiffness samples, (d) bending stiffness histogram, (e) sub-span length ratio (α) samples, and (f) sub-span length ratio (α) histogram.

Table 5. Estimates, nominal values, CIs and errors for the in-plane identification.

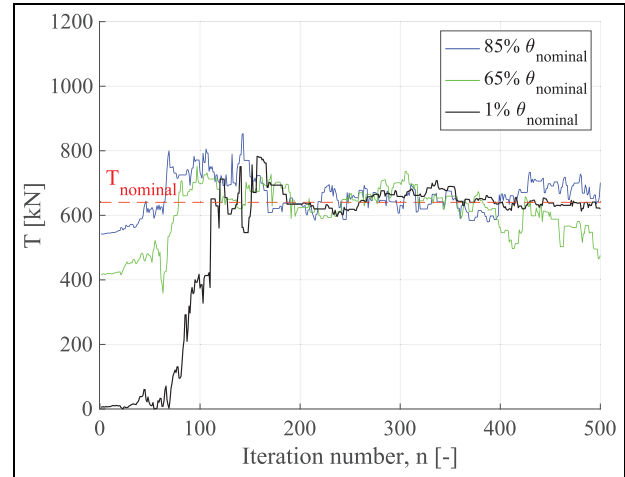| Parameter	Nominal value	Estimated value	CI	Error (%)	CoV (%)
T (kN)	640	670	[543.5, 796.3]	4.69	9.43
EI (kN m^2)	331.4	332	[302.3, 361.7]	0.18	4.47
α (−)	0.352	0.356	[0.349, 0.363]	1.42	0.96

CI: credible interval; EI: uniform bending stiffness.
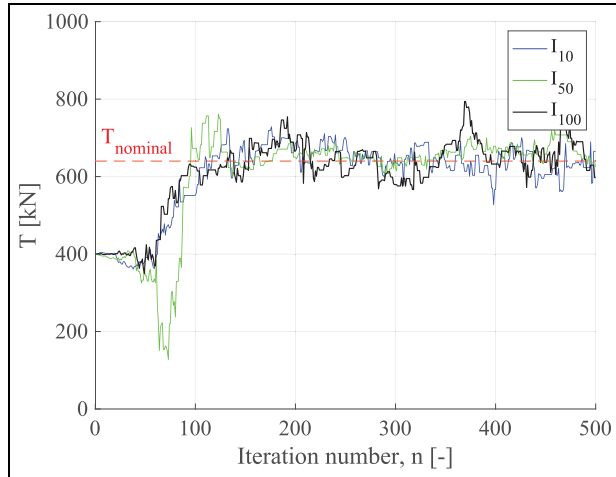
Figure 11. Cable force samples for different ranges of admissible values.

Figure 12. Cable force samples for different initial values. $\theta_{nominal}$ is the vector containing the nominal values of the unknown parameters.

the identification can be considered very efficient even for the definition of the crossing point location.

Convergence rate and accuracy

The influence of the amplitude of the range of admissible values of the parameters and the initial values of the sampling procedure on the convergence rate is examined. The iterations for the identification of the cable force performed by varying the amplitude of the domain are shown in Figure 11. The simulations are performed for three different intervals I_{10}, I_{50} and I_{100} in which the upper (lower) bounds are set respectively to 10 (1/10), 50 (1/50), and 100 (1/100) times the initial values (T_0, EI_0, α_0), The noise intensity and the initial guesses are the same as in the previous section (i.e., Table 4). Interestingly, the convergence rate is not affected by the range of admissible value, as the Burn-in period always lasts about 100 iterations, even for the largest interval (I_{100}). The convergence is faster only when the selected initial values are very close to the nominal ones. Figure 12 shows that when the initial guesses are set to 85% the nominal values the convergence rate drops to 50 iterations as opposed to the 100

iterations needed when the initial values are set to 1% the nominal ones. The initial guesses have a major role in the convergence, contrary to the range of admissible values that does not affect even the accuracy of the identification.

In Table 6 the mean errors and the mean CI amplitudes normalized with respect to the nominal values are computed over 10 simulations performed using different intervals of admissible values. The identifications are carried out with the same initial values and number of iterations as in the previous section. When reducing the amplitude of the domain from I_{100} to I_{10} neither a reduction of the error in the final estimate nor a restriction of the CIs can be observed. Therefore, the intervals should be selected based only on the available information of the unknown parameters, as they should be sufficiently wide to contain the solution to the problem.

The parameter that affects the accuracy of the identification the most is the number of frequencies that are used for the non-linear regression. Table 7 lists the errors and CI amplitudes when 8, 11, or 15 frequencies are used. As expected, when more natural modes are used, the accuracy of the algorithm improves and the

Table 6. Errors and CI amplitudes for different ranges of admissible values (mean values over 10 simulations).

Interval	Parameter	Error (%)	CI Amplitude (%)
I_{100}	T	0.12	26.19
	EI	0.39	11.98
	α	0.15	3.40
I_{50}	T	2.01	24.18
	EI	1.06	10.99
	α	0.46	3.87
I_{10}	T	0.68	26.61
	EI	0.21	12.11
	α	0.10	3.70

CI: credible interval; *EI*: uniform bending stiffness.

Table 7. Errors and CI amplitudes for different numbers of frequencies used in the identifcation (mean values over 10 simulations).

No. frequencies	Parameter	Error (%)	CI Amplitude (%)
8	T	1.84	46.02
	EI	1.93	54.67
	α	1.79	40.68
11	T	1.03	30.36
	EI	0.69	23.05
	α	0.12	8.62
15	T	0.68	26.61
	EI	0.21	12.11
	α	0.10	3.82

CI: credible interval; EI: uniform bending stiffness.

uncertainty of the obtained distribution reduces. The crossing point location α appears quite sensitive to the available quantity of data as the CI amplitudes and the errors reduce by one order of magnitude moving from 8 to 15 frequencies.

The last parameter whose effects are here investigated is the number of samples used after the Burn-in period to build the posterior distributions of the parameters. Three different cases are examined in Table 8. The accuracy of the algorithm does not significantly improve when increasing by one order of magnitude the number of iterations from 100 to 1000. The identification strategy is effective even using only 100 samples. Nevertheless, it is advisable to use at least 1000 samples to have a sufficient resolution in the final distributions.

Algorithm assessment

The performances of the implemented identification strategy in a monitoring environment are assessed through several numerical simulations applied to a cable having the same properties as in Table 3. The

Table 8. Errors and CI amplitudes for different numbers of iterations after the Burn-in period (mean values over 10 simulations).

No. iterations	Parameter	Error (%)	CI Amplitude (%)
100	T	4.42	41.12
	EI	2.73	20.38
	α	1.47	27.07
1000	T	11.93	44.76
	EI	1.15	20.91
	α	0.50	23.19
4000	T	3.47	50.59
	EI	2.01	23.02
	α	6.50	40.41

CI: credible interval; EI: uniform bending stiffness.

identification is performed on 15 simulated eigenfrequencies corrupted by normally distributed noise having a CoV ranging from 0% to 2.5%. Typical values of noise in monitoring stay cables are indeed consistent with the considered range.[32,33] For each noise intensity, the identification is replicated 10 times. The total number of iterations used in the simulations is 5000 with a burn-in period of 2000 jumps. The initial values and explorable intervals of the bending stiffness and the cable force are the same as in the previous section (i.e., initial values as in Table 4 and domains between one-tenth and ten times the initial values). Conversely, the initial guess of α is set closer to the nominal value ($\alpha_0 = 0.33$) and its domain is shrunk to $[0.25, 0.45]$. This choice is made for the sake of avoiding the need for reordering the eigenmodes which is due to large variations of the sub-span lengths, as that may make the identification more involved, especially for highly noised data. The averages of the estimates over the simulations and the associated standard deviations for different noise intensities are depicted in Figure 13(a), (c), and (d) with markers and whiskers respectively. The same statistical quantities are reported in Figure 13(b), (d), and (f) for the CI amplitudes normalized by the associated estimate of each parameter. The results show that the average amplitudes of the CIs and their standard deviations increase almost linearly as the noise intensity becomes larger. On the other hand, the mean estimated values of the cable properties show no bias as the noise increases. The estimated cable forces are more dispersed if compared to the estimated bending stiffness and crossing point position. Overall, the mean estimates are always close to the nominal values and this suggests that the use of several identifications rather than one only is advisable, especially for highly noised frequencies.
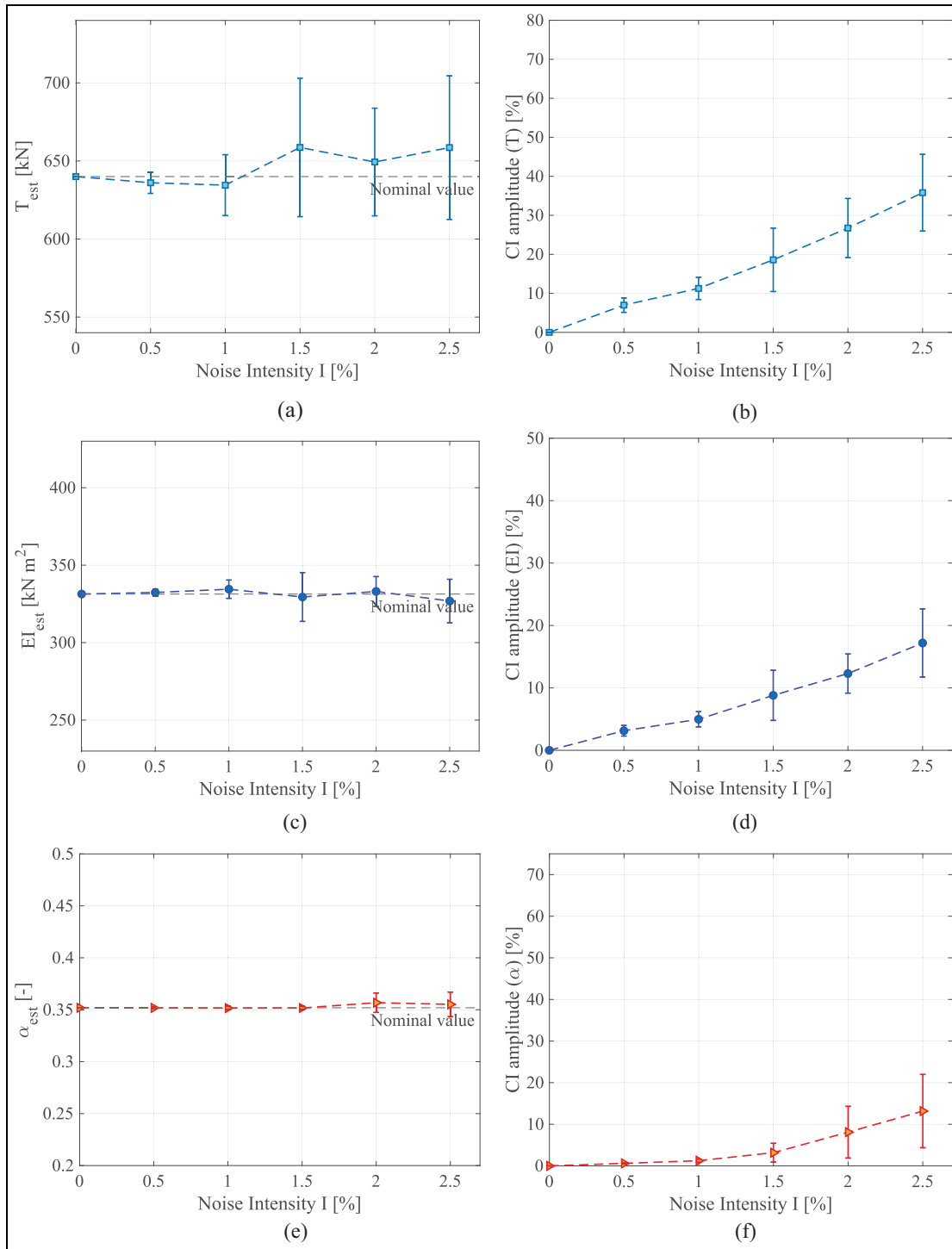
Figure 13. Estimates and credible interval amplitudes at varying noise intensity: (a) Tensile force estimates, (b) tensile force credible interval, (c) bending stiffness estimates, (d) bending stiffness credible interval, (e) sub-span length ratio (α) estimates, and (f) sub-span length ratio (α) credible interval.

**Figure 14.** Tested cable-stayed bridge, Haccourt-Oupeye (Liège).
Source: Picture taken on site on April 26, 2021 by D. Piciucco.

Haccourt bridge application

The dynamic behavior of the cable network described in this document is further investigated through experimental tests aiming at identifying the natural frequencies and mode shapes of the cables of a real bridge. In this section, the experimental campaign, carried out thanks to the partnership with the Wallonia Region, on a cable-stayed bridge (Figure 14) located between Haccourt and Oupeye (Liège, Belgium) is presented. The purpose is to compare the response of a real cable network to the model predictions, computed assuming some given nominal values of the cable forces, bending stiffness, and crossing point location, taken from the available design documentation of the bridge. Since the cable properties (i.e., tension, stiffness, and geometry) might vary through the entire lifetime of the bridges because of environmental effects, aging, changes in loading conditions, and construction errors, their design values might be different from the ones at the time of testing. Therefore, the objective of the following application is to provide a proof of concept of the implemented identification strategy and give statistical information about the actual values of the unknown parameters. More appropriate estimates of the cable properties should indeed further improve the agreement between the model predictions and the real cable network behavior.

Description of the bridge

The tested bridge in Figure 14 is located between Haccourt and Oupeye in the Wallonia region nearby Liège. It is an arch-shaped cable-stayed bridge having a span of 142 m and an arch rise of 23 m. The shop drawings of the bridge, provided by the technicians of the SPW, contained both the geometric characteristics and the expected (nominal) internal actions. The girder of the bridge is characterized by a total width of 23 m divided into three lanes, two road banks and two pedestrian lanes arranged one per side. The arch has a rectangular cross-section of 167×170 mm constituted
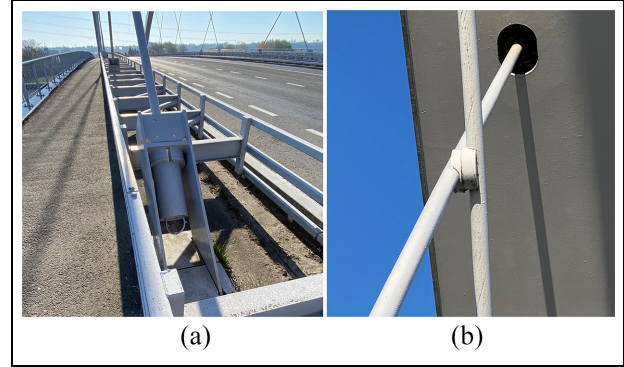
Figure 15. Restraint systems. (a) Anchorage of the cable to the deck and (b) cross connector seen from below.
Source: Pictures taken on site on April 26, 2021 by the author.

by steel plates having a thickness of 30 and 36 mm. The steel arch structure is connected to the girder through a system of 12 stays which constitutes several cable networks with two or three sub-spans. The cables have a diameter $d = 80$ mm with an assumed elastic modulus $E = 168,000$ MPa and a tensile strength of 160 kg/mm^2. The details of the anchorage of the stays to the deck are depicted in Figure 15(a) while the crossing restraints of the cables are in Figure 15(b). Both should allow relative rotation and prevent relative motion in order to be idealized as hinges.

The numbering of the 12 cables on each curb of the bridge is referred to the direction of the cables themselves. The notation is shown in Figure 16. The lengths of the lower, intermediate, and upper spans of the stays extrapolated from the design drawings are summarized in Table 9 (If the length of the intermediate span is zero the cable has only two sub-spans). Those dimensions were provided by the technicians of the SPW who recommended using them only as a reference since they might differ from the actual geometries.

Experimental set-up

The experimental tests involved the measurement of the in-plane natural frequencies of the stays. This was performed by using several piezoelectric accelerometers having a sensitivity of 10,000 mV/g (see Figure 17(a)) placed on each sub-span approximately at midspan. All the sensors were connected by wire to an acquisition system placed inside a van shown in Figure 17(b) and (c). The sensors were oriented transversely to the cable when the measurement of the in-plane vibrations was performed as shown in Fig. 17 (a). The out-of-plane response was also recorded in order to identify and distinguish out-of-plane modes from in-plane resonances. The in-plane time responses induced by the ambient and traffic excitations were registered and stored. The bridge was tested in a low traffic condition,
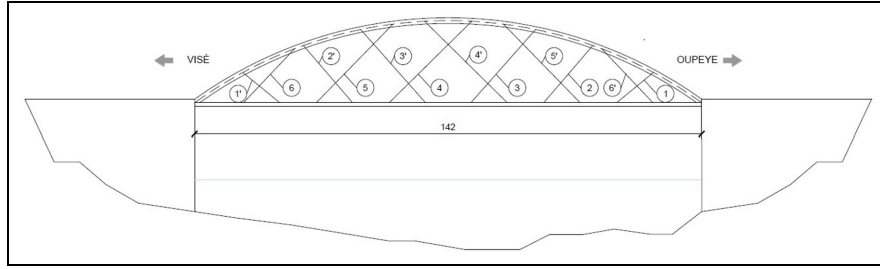
Figure 16. Numbering of the stay cables on the left side of the deck. Dimensions are in meters.

Table 9. Sub-spans' lengths of the tested bridge.

Cable number	Lower span (m)	Intermediate span (m)	Upper span (m)	Total (m)
1	6.65	0	12,25	18.9
2	7.14	14.27	7.79	29.2
3	7.11	14.22	8.82	30.15
4	7	14	5.39	26.4
5	6.81	0	12.88	19.69
6	6.38	0	4.52	10.9

therefore the internal tension of the stays was approximately the one due to the self-weight only. In order to allow the positioning of the sensors the traffic on one lane of the bridge was stopped as shown in Figure 17(a) and a cherry picker was positioned for the installation of the sensors on each sub-span. During the test, four sensors were placed on the cable network constituted by the stays 1 and 6′ having two sub-spans. The accelerometers were placed approximately at mid-span on each cable element and transversely to the stays as in Figure 17(a).

Experimental results

In order to compare the in-plane experimental data with the results of the model described in the previous sections it is possible to make reference to Cable 1 having two sub-spans of lengths $l_1 = 6.65$ m and $l_2 \simeq 2l_1$. The Fast Fourier Transform of the signals (FFT) measured on Cable 1 are depicted in Figure 18. It is worth noting that the third mode (12.63 Hz) generates a significant amplitude of the signal on both the lower and upper span, emphasizing the effect of the bending stiffness. Indeed, the in-plane dynamic behavior, if one neglects the bending stiffness, would be characterized by decoupled mode shapes which mobilize just one of the two sub-spans. Therefore, if the bending stiffness was actually null we would have expected a third mode having high amplitude on one span and negligible amplitude on the other. Similar remarks also apply to higher modes. The experimental results, therefore, confirm that the influence of the bending stiffness in the dynamics of cables having limited lengths cannot be

completely neglected, proving that the proposed model of cables with small bending stiffness is more appropriate than the taut string model.

The in-plane natural frequencies measured on the field are listed in Table 10 together with the ones obtained through FEM analysis, numerical and asymptotic solutions.

### Application of the identification procedure

The experimental tests performed on the stays 1 and 6′ of the Haccourt bridge proved good agreement between the predicted in-plane natural frequencies and the observed data. However, the results provided by the models can be further improved by identifying the actual cable forces, crossing point location, and bending stiffness of the tested network through an inverse analysis applied to the experimental frequencies.

Therefore, the in-plane observed eigenfrequencies are used to estimate the cable properties of the stay n.1. The proposed Bayesian algorithm, applied to the experimental data already presented in Table 10, should provide the most likely values of T, EI, and α. The difficulty in identifying higher frequencies from the experimental spectrum makes it necessary to use just six frequencies for the identification. However, more generally, as far as the accuracy of the measures increases, more frequencies can be used to have even better estimates of the unknown structural parameters.

The cable length l and the mass per unit length m are assumed to be known and the MH sampling procedure is performed by setting the initial value of the
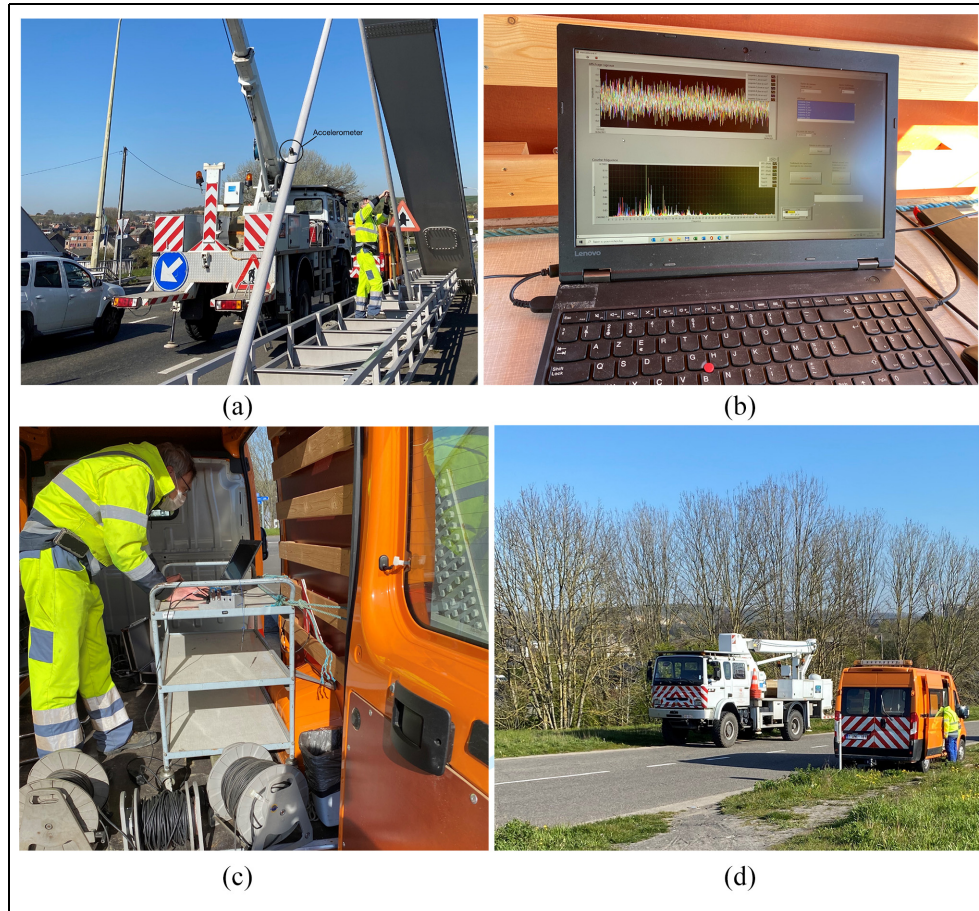
Figure 17. Experimental equipment: (a) In-plane set-up, (b) PC, (c) acquisition point, and (d) truck and van before the installation.
Source: Pictures taken on site on April 26, 2021 by D. Piciucco.
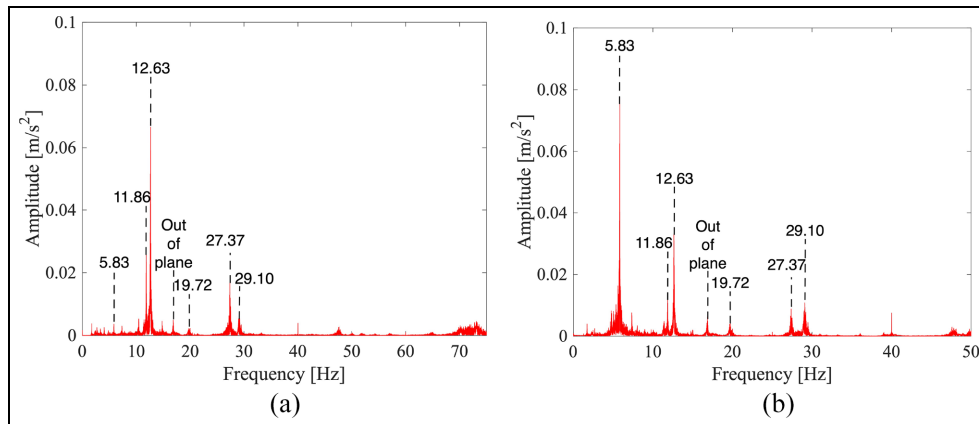
Figure 18. Experimental frequency domain signal (FFT) measured on the upper and lower spans of the cable 1. (a) FFT, lower span, and (b) FFT, upper span.

unknown parameters to the nominal values reported in the design drawings (Table 11). This is indeed in the spirit of the Bayesian approach since the proposed identification procedure allows to introduce available information in the problem by using informative priors or by setting initial values close to the expected ones. In a monitoring environment, initial estimates of the cable tension, bending stiffness, and crossing point

Table 10. In-plane eigenfrequencies of the cable n.1 having $\varepsilon_1 = 0.059$, $\varepsilon_2 = 0.108$.

Mode no.	Numerical results (Hz)	Asymptotic results (Hz)	FEM results (Hz)	Experimental data (Hz)
1	5.79	5.78	5.74	5.83
2	11.15	11.17	11.07	11.86
3	12.39	12.35	12.30	12.63
4	19.47	19.55	19.32	19.72
5	25.66	25.97	25.47	27.37
6	28.71	29.18	28.49	29.09

FEM: Finite Element Method.

Table 11. Initial values of the unknown parameters for the in-plane identification in the Haccourt bridge.

T_0 (kN)	EI_0 (kN m^2)	α_o (–)
640	331.4	0.352

Table 12. Estimates, nominal values, and CIs for the in-plane identification in the Haccourt bridge.

Unknowns variables	Estimated value	Nominal value	CI
T (kN)	739.1	640	[455.3, 1023.8]
EI (kN m^2)	315.9	331.4	[96, 595]
α (–)	0.339	0.352	[0.301, 0.377]

CI: credible interval; EI: uniform bending stiffness.

position can be easily obtained from past monitoring activities or found in the available documentation.

The upper and lower bounds of the explorable intervals are set as one-tenth and ten times the initial values for the tension and the bending stiffness while α is limited to 0.5. Available information on the monitored structure could be used to set even narrower intervals, especially for α. Large changes of the sub-span lengths indeed, may induce reordering of the eigenmodes because of the wavelength variation. This effect slows down the identification and makes the iterative sampling procedure more complicated.

The PDF of the parameters obtained after 6000 iterations are depicted in Figure 19, while the final estimates and CIs are reported in Table 12. All the parameters are very well estimated; the distributions are bell-shaped with sharp peaks. The bending stiffness estimate turns out to be very close to the nominal value while the estimated cable tension is higher than expected. This means that the discrepancies in terms of eigenfrequencies, though small, between the model and the tested network are mainly due to an underestimation of the cable force. The 15% difference between the estimated value of the cable force and its design value can be associated with two main sources of uncertainties. The design value of the tension is the planned tension (at design stage) corresponding to a load case with self-weight only. Nothing guarantees that all stay cables could have been installed with the planned axial force. Moreover, at the time of testing one lane of the bridge was open to the traffic and a cherry picker and a truck were placed near the tested cable network. It has already been shown in Tab.7, that the amplitude of the credible intervals could be improved if more than six eigenfrequencies were measured. In fact, one of the

merits of the proposed Bayesian regression inference is to duly inform about the quality of the identification process.

The discrete values of the first six in-plane numerical eigenfrequencies before and after identification, are listed in Table 13. The numerical solutions match the first six experimental natural frequencies and, comparing the updated eigenfrequencies to the ones computed before identification, a relevant improvement of the predicted fifth mode can be observed at the price of a very slight worsening of the fundamental frequency. The root mean square error (RMSE) of the predicted eigenfrequencies indeed drops from 0.785 before identification down to 0.324 after identification. This means that, even if the Bayesian procedure is not based on a minimization of the RMSE, it also involves a reduction of the error itself, confirming the appropriateness of the identification strategy.

Conclusions

In this work, the in-plane dynamic behavior of a cable network constituted by crossing stays has been analyzed for the implementation of an identification procedure that aims at defining cable properties from a given set of observed eigenfrequencies. First, the direct analysis of the proposed structural scheme has been developed through analytical models whose results have been compared to the FEM outcomes. Then, an identification procedure based on Bayesian non-linear regression has been implemented for the estimation of cable forces, bending stiffness, and the crossing point
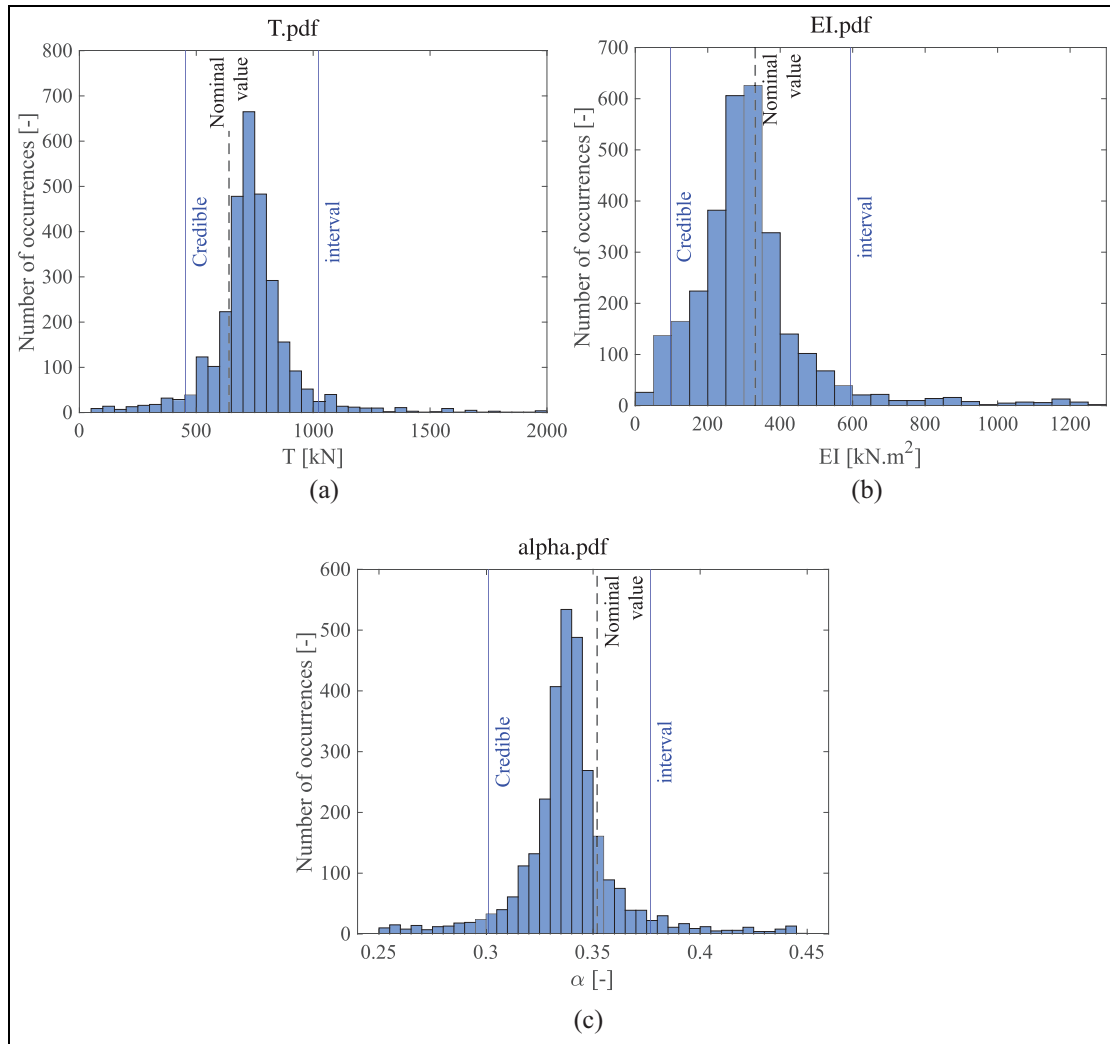
Figure 19. Histograms, In-plane identification in the Haccourt bridge. (a) Tensile force histogram, (b) bending stiffness histogram, and (c) sub-span length ratio (α) histogram.

Table 13. In-plane eigenfrequencies before and after identification. In parenthesis the relative error with respect to the experimental results.

Frequencies	Experimental data (Hz)	Before identification (Hz)	After identification (Hz)
f_1	5.83	5.79 (0.75%)	6.05 (3.70%)
f_2	11.86	11.15 (5.94%)	12.12 (2.17%)
f_3	12.63	12.39 (1.90%)	13.07 (3.42%)
f_4	19.72	19.47 (1.25%)	19.98 (1.31%)
f_5	27.37	25.66 (6.23%)	27.48 (0.40%)
f_6	29.09	28.71 (1.30%)	29.58 (1.67%)

location of the cable network. Theoretical studies have been supported by experimental tests performed on a real cable-stayed bridge whose results have been used both to better understand the dynamic behavior of the structural scheme and to provide a proof of concept of the identification strategy.

More specifically, the results presented in the document clearly highlight that:

- Analytical models have some advantages when compared to the FEM for the analysis of cable networks. They provide mathematical solutions to the dynamic problem that are useful to understand the influence of each governing parameter. Well-defined assumptions are also useful to engineers to define the validity and applicability of the analytical methods.
- Closed form asymptotic solutions are useful to understand the limit behavior of cable structures, providing also reliable results when the bending stiffness is small. They are particularly useful for the definition of the independent groups of parameters to be identified in the inverse problem;
- The dynamic behavior of a real cable network, as the tested one, can be better captured by a cable model which takes into account the small bending stiffness rather than a taut string model;
- The proposed identification tool can be used to refine initial estimates of the crossing point position of the cables;
- The identification procedure provides unbiased estimates of the cable properties even for large values of noise;
- The accuracy of the identification strategy can be improved by increasing the number of eigenfrequencies used for the non-linear regression and shrinking the explorable space of the cable parameters.
- For highly noised frequencies the restriction of the explorable interval for the connector position is recommended to avoid reordering of the eigenmodes;
- At large noise intensity the accuracy of the predictions can be improved by computing the mean estimates of the cable properties over several simulations;
- The proposed algorithm works and can be used also in a real monitoring environment;
- A more accurate model could be implemented as in Foti et al.[18] by considering the end-restraints as rotational and translational springs whose stiffness are additional unknowns in the identification process.

Author's Note

Margaux Geuzaine is now affiliated at NatHaz Modeling Laboratory, University of Notre Dame, Indiana, USA.

Acknowledgements

Declaration of conflicting interests

Funding

ORCID iD

Margaux Geuzaine https://orcid.org/0000-0001-7454-7816

References

1. Geuzaine M, Foti F and Denoël V. Minimal requirements for the vibration-based identification of the axial force, the bending stiffness and the flexural boundary conditions in cables. *J Sound Vib* 2021; 511(November 2020): 116326.
2. Caetano E. *Cable Vibrations in cable-stayed bridges*, Zurich, Switzerland, IABSE, 2007.
3. Xie X, Hu X, Peng J, et al. Refined modeling and free vibration of two-span suspended transmission lines. *Acta Mech* 2017; 228(2): 673–681.
4. Caracoglia L and Jones NP. In-plane dynamic behavior of cable networks. Part 1: Formulation and basic solutions. *J Sound Vib* 2005; 279(3–5): 969–991.
5. Younespour A and Cheng S. In-plane modal responses of two-cable networks considering cable bending stiffness effect. *Eng Struct* 2021; 230(April 2020): 111691.
6. Younespour A and Cheng S. In-plane modal behavior of a single shallow flexible cable with an intermediate transverse elastic support. *J Sound Vib* 2022; 534(September 2021): 117093.
7. Di F, Chen L and Sun L. Free vibrations of hybrid cable networks with external dampers and pretensioned cross-ties. *Mech Syst Signal Process* 2021; 156: 107627.
8. Ahmad J. In-plane linear dynamic behavior and impact of key system parameters of low-sagged cable network. *J Sound Vib* 2021; 490: 115728. 10.1016/j.jsv.2020.115728.
9. Jing H, He X, Zou Y, et al. In-plane modal frequencies and mode shapes of two stay cables interconnected by uniformly distributed cross-ties. *J Sound Vib* 2018; 417: 38–55.
10. Ehsan F and Scanlan RH. Damping stay cables with ties. In: *Proceedings of the 5th US-Japan workshop on aerodynamics*, Tsukuba, Ibaraki, 1989, pp. 203–217. Japan: Publick Work Research Institute.
11. Graff K. *Wave motion in elastic solids*. Dover Books on Physics Series, Dover Publications, 1991. https://books.google.it/books?id=5cZFRwLuhdQC
12. Denoël V and Canor T. Patching asymptotics solution of a cable with a small bending stiffness. *J Struct Eng* 2013; 139(2): 180–187.
13. Foti F and Martinelli L. Finite element modeling of cable galloping vibrations—Part I: Formulation of mechanical

and aerodynamic co-rotational elements. *Arch Appl Mech* 2018; 88(5): 645–670.

14. Foti F and Martinelli L. Finite element modeling of cable galloping vibrations. Part II: Application to an iced cable in 1:2 multiple internal resonance. *JVC/Journal Vib Control* 2018; 24(7): 1322–1340.
15. Casas J. A combined method for measuring cable forces: the cable-stayed Alamillo Bridge, Spain. *Struct Eng Int 1994* 1994; 4(4): 235–240.
16. Gentile C. Deflection measurement on vibrating stay cables by non-contact microwave interferometer. *NDT E Int* 2010; 43(3): 231–240.
17. Bao Y, Shi Z, Beck JL, et al. Identification of time-varying cable tension forces based on adaptive sparse time-frequency analysis of cable vibrations. *Struct Control Heal Monit* 2017; 24(3): 1–17.
18. Foti F, Geuzaine M and Denoël V. On the identification of the axial force and bending stiffness of stay cables anchored to flexible supports. *Appl Math Model* 2021; 92: 798–828.
19. Furukawa A, Yamada S and Kobayashi R. Tension estimation methods for two cables connected by an intersection clamp using natural frequencies. *J Civ Struct Heal Monit* 2022; 12(2): 339–360.
20. Thierry A, Patrice T, Denoël V, et al. An integrated solution for tension monitoring in bridge hangers and stay cable by means of vibration measurement. In: *IABSE congress Ghent 2021 "Structural Engineering for Future Societal Needs"*, Ghent, pp. 511–517.
21. Geuzaine M, Foti F, Verstraelen E, et al. Development of a general monitoring program for bridge stays and hangers in Wallonia, Belgium. In: *Second international symposium on dynamics and aerodynamics of cables – ISDAC 2021*, Stavanger, pp. 115–121.
22. Irvine H and Cughey T. The linear theory of free vibrations of a suspended cable. *R Soc* 1974; 341: 299–315.
23. Denoël V and Detournay E. Multiple scales solution for a beam with a small bending stiffness. *J Eng Mech* 2010; 136(1): 69–77.
24. Chopra AK. *Dynamics of structures: theory and applications to earthquake engineering*. Englewood Cliffs, New Jersey: Prentice Hall, 1995.
25. Soe TTT and Khaing SY. Evaluation of cable force changes effects on cable stayed bridge. *Civ Eng J* 2020; 6(11): 2159–2174.
26. Talebinejad I, Fischer C and Ansari F. Numerical evaluation of vibration-based methods for damage assessment of cable-stayed bridges. *Comput Civ Infrastruct Eng* 2011; 26(3): 239–251.
27. Clyde M, Cetinkaya-Rundel M, Rundel C, et al. An introduction to Bayesian thinking. A Companion to the Statistics with R Course, 2019.
28. Koehrsen W. Introduction to Bayesian linear regression. Online referencing, https://towardsdatascience.com/introduction-to-bayesian-linear-regression-e66e60791ea7 (2018, accessed 25 October 2021).
29. Yildirim I. Bayesian inference: Metropolis-Hastings sampling. Technical Report, 2012.
30. Hespanhol L, Vallio CS, Costa LM, et al. Understanding and interpreting confidence and credible intervals around effect estimates. *Brazilian J Phys Ther* 2019; 23(4): 290–301.
31. Allison PD. *Missing data*. Thousand Oaks, CA: Sage publications, 2001.
32. Van Overschee P and De Moor B. Subspace algorithms for the stochastic identification problem. *Automatica* 1993; 29(3): 649–660.
33. Piersol AG and Paez TL (eds.) *Harris' shock and vibration handbook*. 6th ed. New York: McGraw-Hill Education, 2010.

Appendix A

In this appendix, additional details regarding the direct analysis of the in-plane problem are reported. The non-zero entries of the boundary condition matrix $\boldsymbol{B}$ (8×8) are listed here, exploiting the definition of the variables z_1, z_2, z_3 and z_4 (see Equations (16) and (17)) which significantly simplify their expressions. Each entry is indicated as $B_{i,j}$ with i and j denoting the ith row and the jth column.

$$B_{1,2} = 1 \tag{A1}$$
$$B_{1,3} = 1 \tag{A2}$$
$$B_{1,4} = \exp(-z_2) \tag{A3}$$
$$B_{2,1} = \sin(z_1) \tag{A4}$$
$$B_{2,2} = \cos(z_1) \tag{A5}$$
$$B_{2,3} = \exp(-z_2) \tag{A6}$$
$$B_{2,4} = 1 \tag{A7}$$
$$B_{3,6} = 1 \tag{A8}$$
$$B_{3,7} = 1 \tag{A9}$$
$$B_{3,8} = \exp(-z_4) \tag{A10}$$
$$B_{4,5} = \sin(z_3) \tag{A11}$$
$$B_{4,6} = \cos(z_3) \tag{A12}$$
$$B_{4,7} = \exp(-z_4) \tag{A13}$$
$$B_{4,8} = 1 \tag{A14}$$
$$B_{5,1} = -\varepsilon_1^2 z_1^2 \sin(z_1) \tag{A15}$$
$$B_{5,2} = -\varepsilon_1^2 z_1^2 \cos(z_1) \tag{A16}$$
$$B_{5,3} = \varepsilon_1^2 z_2^2 \exp(-z_2) \tag{A17}$$
$$B_{5,4} = \varepsilon_1^2 z_2^2 \tag{A18}$$
$$B_{6,5} = -\varepsilon_2^2 z_3^2 \sin(z_3) \tag{A19}$$
$$B_{6,6} = -\varepsilon_2^2 z_3^2 \cos(z_3) \tag{A20}$$

$$B_{6,7} = \varepsilon_2^2 z_4^2 \exp(-z_4) \qquad (A21)$$

$$B_{6,8} = \varepsilon_2^2 z_4^2 \qquad (A22)$$

$$B_{7,1} = \varepsilon_1 z_1 \qquad (A23)$$

$$B_{7,3} = -\varepsilon_1 z_2 \qquad (A24)$$

$$B_{7,4} = \varepsilon_1 z_2 \exp(-z_2) \qquad (A25)$$

$$B_{7,5} = \varepsilon_1 z_3 \qquad (A26)$$

$$B_{7,7} = -\varepsilon_1 z_4 \qquad (A27)$$

$$B_{7,8} = \varepsilon_1 z_4 \exp(-z_4) \qquad (A28)$$

$$B_{8,2} = -\varepsilon_1^2 z_1^2 \qquad (A29)$$

$$B_{8,3} = \varepsilon_1^2 z_2^2 \qquad (A30)$$

$$B_{8,4} = \varepsilon_1^2 z_2^2 \exp(-z_2) \qquad (A31)$$

$$B_{8,6} = a\varepsilon_1^2 z_3^2 \qquad (A32)$$

$$B_{8,7} = -a\varepsilon_1^2 z_4^2 \qquad (A33)$$

$$B_{8,8} = -a\varepsilon_1^2 z_4^2 \exp(-z_4) \qquad (A34)$$

In-plane perturbation approach

The non-zero entries of the matrices $\boldsymbol{B}_{(0)}$, $\boldsymbol{B}_{(1)}$, and $\boldsymbol{B}_{(2)}$ are here reported and denoted as $\boldsymbol{B}_{(0)i,j}$, $\boldsymbol{B}_{(1)i,j}$, and $\boldsymbol{B}_{(2)i,j}$ ($i,j = 1, \ldots, 8$) with the same notation as before. The entries of the leading order $\boldsymbol{B}_{(0)}$ matrix are listed from Equations (A35) to (A50).

$$B_{(0)1,2} = 1 \qquad (A35)$$

$$B_{(0)1,3} = 1 \qquad (A36)$$

$$B_{(0)2,1} = \sin(a\omega_{(0)}) \qquad (A37)$$

$$B_{(0)2,2} = \cos(a\omega_{(0)}) \qquad (A38)$$

$$B_{(0)2,4} = 1 \qquad (A39)$$

$$B_{(0)3,4} = 1 \qquad (A40)$$

$$B_{(0)4,6} = 1 \qquad (A41)$$

$$B_{(0)4,7} = 1 \qquad (A42)$$

$$B_{(0)5,5} = -\sin(-\omega_{(0)}) \qquad (A43)$$

$$B_{(0)5,6} = \cos(-\omega_{(0)}) \qquad (A44)$$

$$B_{(0)5,8} = 1 \qquad (A45)$$

$$B_{(0)6,8} = 1 \qquad (A46)$$

$$B_{(0)7,3} = -1 \qquad (A47)$$

$$B_{(0)7,7} = -1/a \qquad (A48)$$

$$B_{(0)8,3} = 1 \qquad (A49)$$

$$B_{(0)8,7} = -1/a \qquad (A50)$$

The non-zero entries of the first order matrix $\boldsymbol{B}_{(1)}$ are reported in the following Equations (A51) to (A56).

$$B_{(1)2,1} = a\omega_{(1)} \cos(a\omega_{(0)}) \qquad (A51)$$

$$B_{(1)2,2} = -a\omega_{(1)} \sin(a\omega_{(0)}) \qquad (A52)$$

$$B_{(1)5,5} = \omega_{(1)} \cos(-\omega_{(0)}) \qquad (A53)$$

$$B_{(1)5,6} = -\omega_{(1)} \sin(-\omega_{(0)}) \qquad (A54)$$

$$B_{(1)7,1} = \omega_{(0)} \qquad (A55)$$

$$B_{(1)7,5} = \omega_{(0)}/a \qquad (A56)$$

The entries of the matrix $\boldsymbol{B}_{(2)}$ are reported in the Equations (A57) to (A74) hereafter.

$$B_{(2)2,1} = \left(-\alpha^2\omega_{(0)}^3 + 2\omega_{(2)} - 4\alpha\omega_{(2)} + 2\alpha^2\omega_{(2)}\right)\frac{\cos(\omega_{(0)})}{2(\alpha-1)^2} - \frac{\omega_1^2 \sin(\omega_0)}{2} \qquad (A57)$$

$$B_{(2)2,2} = -\left(-\alpha^2\omega_0^3 + 2\omega_2 - 4\alpha\omega_2 + 2\alpha^2\omega_2\right)\frac{\sin(\omega_0)}{2(\alpha-1)^2} - \frac{\omega_1^2 \cos(\omega_0)}{2} \qquad (A58)$$

$$B_{(2)3,1} = -\omega_{(0)}^2 \sin(a\omega_{(0)}) \qquad (A59)$$

$$B_{(2)3,1} = -\omega_{(0)}^2 \cos(a\omega_{(0)}) \qquad (A60)$$

$$B_{(2)3,5} = \omega_{(0)}^2 \qquad (A61)$$

$$B_{(2)5,5} = ((2\omega_{(2)} - \omega_{(0)}^3) \cos(\omega_{(0)}) + \omega_{(1)}^2 \sin(\omega_0))/2 \qquad (A62)$$

$$B_{(2)5,6} = ((2\omega_{(2)} - \omega_{(0)}^3) \sin(\omega_{(0)}) - \omega_{(1)}^2 \cos(\omega_{(0)}))/2 \qquad (A63)$$

$$B_{(2)6,5} = \omega_{(0)}^2 \sin(-\omega_{(0)}) \qquad (A64)$$

$$B_{(2)6,6} = -\omega_{(0)}^2 \cos(-\omega_{(0)}) \qquad (A65)$$

$$B_{(2)6,6} = \omega_{(0)}^2 \qquad (A66)$$

$$B_{(2)7,1} = \omega_{(1)} \qquad (A67)$$

$$B_{(2)7,3} = -\omega_{(0)}^2/2 \qquad (A68)$$

$$B_{(2)7,5} = \omega_{(1)}^2 \qquad (A69)$$

$$B_{(2)7,7} = -\omega_{(0)}^2/2a \qquad (A70)$$

$$B_{(2)8,2} = \omega_{(0)}^2 \qquad (A71)$$

$$B_{(2)8,3} = \omega_{(0)}^2 \qquad (A72)$$

$$B_{(2)8,6} = \omega_{(0)}^2/a \qquad (A73)$$

$$B_{(2)8,7} = -\omega_{(0)}^2/a \qquad (A74)$$

Appendix B

In this appendix, the solution of the in-plane eigenvalue problem through a perturbation approach is described in detail. The system (24) is solved through a cascade approach starting from the unperturbed problem (i.e., without bending stiffness) and then searching for the first and second order corrections.

Leading order problem

The starting point of the procedure is the solution of the first equation of the system (24). This means looking for leading order eigenvalues $\omega_{(0),k}$ and eigenvectors $\varphi_{(0),k}$ of the $\boldsymbol{B}_{(0)}$ matrix. The frequencies $\omega_{(0),k}$ are therefore the roots of the Equation (B1).

$$\det[\boldsymbol{B}_{(0)}(\omega_{(0)})] = 0 \qquad (B1)$$

$$\omega_{(0),k} = \frac{k\pi}{a} \quad \text{or} \quad \omega_{(0),k} = k\pi \qquad (B2)$$

The solutions (B2) are the non-dimensional counterparts of the eigenfrequencies of the taut string in-plane vibrations, with a being the ratio of the two sub-spans length ($a = 1 - \alpha/\alpha$). The corresponding leading order left and right eigenvectors $\varphi_{(0),k}$ and $\boldsymbol{\delta}_{(0),k}$ are:

$$\varphi_{(0),k} = (1,0,0,0,0,0,0,0)^T \qquad (B3)$$

or

$$\varphi_{(0),k} = (0,0,0,0,1,0,0,0)^T \qquad (B4)$$

and

$$\boldsymbol{\delta}_{(0),k} = \left(1, -(-1)^k, (-1)^k, 0, 0, 0, 1/2, -1/2\right) \qquad (B5)$$

or

$$\boldsymbol{\delta}_{(0),k} = \left(0,0,0, -(-1)^k, 1, -1, -\frac{a}{2}(-1)^k, -\frac{a}{2}(-1)^k\right) \qquad (B6)$$

First order correction

Once the leading order solutions are known, the first-order correction of the eigenfrequencies can be

determined through simple computations. Pre-multiplication of the second equation of the system (24) by the left eigenvectors $\boldsymbol{\delta}_{(0),k}$ corresponding to each leading order eigenfrequency (B2) yields:

$$\boldsymbol{\delta}_{(0),k}^T \boldsymbol{B}_{(1)}(\omega_{(0),k}, \omega_{(1),k}) \varphi_{(0),k} = 0 \qquad (B7)$$

whose solutions $\omega_{(1),k}$ are:

$$\omega_{(1),k} = \frac{k\pi}{2a^2} \quad \text{or} \quad \omega_{(1),k} = \frac{k\pi}{2} \qquad (B8)$$

Substitution of the Equations (B2) to (B4) and (B8) in the second order problem, that is, second equation of the system (24), leads to the following equation:

$$\boldsymbol{B}_{(0)}(\omega_{(0),k}) \varphi_{(1),k} = -\boldsymbol{B}_{(1)}(\omega_{(0),k}, \omega_{(1),k}) \varphi_{(0),k} \qquad (B9)$$

that can be solved for $\varphi_{(1),k}$, yielding:

$$\varphi_{(1),k} = \frac{k\pi}{2}\left(0, -\frac{1}{a}, \frac{1}{a}, 0, \cot\left(\frac{k\pi}{a}\right), -1, 1, 0\right)^T \qquad (B10)$$

or

$$\varphi_{(1),k} = \frac{k\pi}{2}\left(\cot(ak\pi), -\frac{1}{a}, \frac{1}{a}, 0, 0, 1, -1, 0\right)^T \qquad (B11)$$

Second order correction

Once both the first order and leading order solutions are known, the equation of the second order problem pre-multiplied by $\boldsymbol{\delta}_{(0),k}^T$ yields the scalar Equation (B12) from which the second order correction of the eigenfrequencies $\omega_{(2),k}$ can be computed.

$$\boldsymbol{\delta}_{(0),k}^T \boldsymbol{B}_{(1)}(\omega_{(0),k}, \omega_{(1),k}) \varphi_{(1),k}$$
$$+ \boldsymbol{\delta}_{(0),k}^T \boldsymbol{B}_{(2)}(\omega_{(0),k}, \omega_{(1),k}, \omega_{(2),k}) \varphi_{(0),k} = 0 \qquad (B12)$$

$$\omega_{(2),k} = \frac{k\pi}{4a^2}\left(1 + 2k^2\pi^2 + k\pi \cot\left(\frac{k\pi}{a}\right)\right) \qquad (B13)$$

or

$$\omega_{(2),k} = \frac{k\pi}{4}\left(1 + 2k^2\pi^2 + k\pi \cot(ak\pi)\right) \qquad (B14)$$

Replacing Equations (B2) to (B4), (B8), (B9), (B10), and (B13) in the third equation of the system (24), one gets the second order correction of the eigenvectors $\varphi_{(2),k}$:

$$\boldsymbol{\varphi}_{(2),k} = \frac{k\pi}{4a}\left(0,\ -\frac{r}{a},\frac{r}{a},0,p,\ -r,r,0\right)^{T} \qquad \text{(B15)}$$

with

$$p = r\cot\left(\frac{k\pi}{a}\right) - \left(\frac{k\pi}{a}\right)\left(1 + \cot^{2}\left(\frac{k\pi}{a}\right)\right) \qquad \text{(B16)}$$

and

$$r = 1 + k\pi\cot\left(\frac{k\pi}{a}\right) \qquad \text{(B17)}$$

or

$$\boldsymbol{\varphi}_{(2),k} = \frac{k\pi}{4}\left(q,\ -\frac{s}{a},\frac{s}{a},0,0,\ -s,s,0\right)^{T} \qquad \text{(B18)}$$

with

$$q = \frac{(1-2a)k\pi + s\ \sin(ak\pi)}{2a\ \sin^{2}(ak\pi)} \qquad \text{(B19)}$$

and

$$s = 1 + k\pi\cot(ak\pi) \qquad \text{(B20)}$$

The expressions of all the coefficients $\omega_{(n)}$ being known, the second order eigenfrequencies can be computed according to Equation (20).